One-step induction of human GABAergic neurons promotes presynaptic development & synapse maturation

Torben W. van Voorst[1,+], Maaike A. van Boven [1,+], Kevin I. Marinus[2,+], Jennifer M. Colón-Mercado[3], Jule Schretzmeir[1], Carolin Haag[1,4], Ruud F. Toonen[1,4], Frank Koopmans[2], Michael E. Ward[3], August B. Smit[2], Ronald E. van Kesteren[2], Matthijs Verhage[1,4,5], L. Niels Cornelisse[1,5,#]

[1]Department of Functional Genomics, Center for Neurogenomics and Cognitive Research (CNCR), VU University Amsterdam, de Boelelaan 1100, 1081 HZ Amsterdam, The Netherlands.

[2]Department of Molecular and Cellular Neurobiology, Center for Neurogenomics and Cognitive Research (CNCR), VU University Amsterdam, de Boelelaan 1100, 1081 HZ Amsterdam, The Netherlands.

[3]National Institute of Neurological Disorders and Stroke, National Institutes of Health, 9000 Rockville Pike, Bethesda, MD, USA

[4]Neurospector, de Boelelaan 1100, 1081 HZ Amsterdam, The Netherlands.

[5]Department of Human Genetics, Amsterdam UMC – location VU University Amsterdam, de Boelelaan 1100, 1081 HV Amsterdam, The Netherlands.

[+] *Authors contributed equally*

[#] *Correspondence: l.n.cornelisse@vu.nl*

Abstract (174 words)

Human induced pluripotent stem cells (iPSCs) present a powerful approach to study human brain physiology and disease, yet robust, pure GABAergic induction has remained difficult. Here we present improved, single-step, transposon-based GABAergic induction with Ascl1/Dlx2, which yields pure GABAergic neurons, in contrast to lentiviral approaches, and was tested across three independent iPSC lines. Proteomic and electrophysiological characterization at different developmental time points showed that these neurons gain a proteomic profile that maps to different cortical interneuron subtypes, particularly VIP+ interneurons, and display typical GABAergic synaptic properties, producing large, synchronous and picrotoxin-sensitive currents. During early development synaptic strength increased threefold, which was accompanied by enhanced expression of multiple GABA-specific presynaptic gene sets, but few changes in postsynaptic gene sets. Synaptic strength continued to improve during late development but with only minor proteomic changes. Co-

seeding with NGN2 neurons created stable networks of predefined excitation/inhibition ratios, with corresponding synapse ratios. Taken together, transposon-based GABAergic induction yields pure, mature GABAergic neurons suitable for studying gene sets involved in synaptic maturation and to build excitation/inhibition networks for disease modelling.

Keywords (max 10)

Induced pluripotent stem cells, induced GABAergic neurons, Transposon, Synaptic maturation, Ascl1, Dlx2, Autaptic neurons, Proteomics, Patch-clamp, Excitation/inhibition

Introduction

Human induced pluripotent stem cell (iPSC)-derived models provide a promising platform for studying human brain physiology and pathology. iPSCs can be generated from patient-derived tissue or blood to better reflect the human genetics and (patho)physiology compared to commonly employed rodent models (Breschi *et al*, 2017; Gharib & Robinson-Rechavi, 2011; Hoffman *et al*, 2019). GABAergic dysfunction and excitation/inhibition (E/I) disbalance have been implicated in many neurodevelopmental and neurodegenerative disorders (Busche *et al*, 2008; Foss-Feig *et al*, 2017; Nelson & Valakh, 2015; Palop *et al*, 2007a; Rubenstein & Merzenich, 2003; Sohal & Rubenstein, 2019). In recent years, various strategies have been developed for generating iPSC-derived GABAergic neurons, but robust, pure GABAergic induction remains challenging. Directed differentiation, which employs signalling molecules to mimic neurodevelopment (Liu *et al*, 2013; Maroof *et al*, 2013; Nicholas *et al*, 2013), yields both glutamatergic and GABAergic neurons, but these type of inductions often generate inconsistent E/I ratios, tend to yield heterogeneous and immature neuronal populations and are costly and time-consuming (Engle *et al*, 2018). Rapid differentiation approaches rely on overexpression of key transcription factors, such as Ascl1 and Dlx2 for GABAergic differentiation (Mossink *et al*, 2022; Yang *et al*, 2017) and often rely on lentiviral delivery of transgenes. However, such approaches have several limitations: (1) they require multiple vectors when delivering multiple transgenes due to the size cap of ~8 kb, (2) they pose a risk of disrupting host genes (Baum, 2007), and (3) they are susceptible to epigenetic silencing during prolonged iPSC culturing (Cabrera *et al*, 2022; Wolf & Goff, 2009; Yao *et al*, 2004). To overcome these challenges, TALEN- and CRISPR-based gene editing (Miller *et al*, 2011) have been used to target the transgenes to the *AAVS1* safe harbour locus (Peitz *et al*, 2020; Schmid *et al*, 2021). While this ensures stable transgene expression, allows for delivery of multiple genes in a single construct, and minimizes off-target effects,

it is time and resource-consuming due to the need for clonal expansion and extensive validation of every iPSC line used in a study (Lombardo *et al*, 2011).

The PiggyBac transposon system has emerged as a gene-delivery tool that overcomes most of these limitations. Unlike lentiviral systems, transposons enable stable genomic integration of large genetic constructs up to 200 kb (Li *et al*, 2013) through a "cut-and-paste" mechanism (Wilber *et al*, 2007), which enables delivery of multiple transgenes in a single construct. Additionally, transposon-delivered transgenes are less prone to silencing than lentivirally delivered transgenes (Ng *et al*, 2021) and the increased packing capacity permits the inclusion of epigenetic regulators to further diminish silencing. Compared to safe-harbour insertion of transgenes, the delivery of a transposon cassette is a simpler, single-step process applicable to multiple iPSC lines in parallel and allows the use of a polyclonal population for most use cases, eliminating the need for thorough validation, thereby accelerating experimental timelines.

Here, we characterize PiggyBac transposon-based overexpression of *Ascl1* and *Dlx*2 (PB-AD) for GABAergic neuronal induction and benchmark this against established GABAergic induction methods. PB-AD-based induction results in pure GABAergic differentiation across different genetic backgrounds, with proteomic signatures characteristic of several human cortical interneuron types, with the strongest resemblance to VIP^+ interneurons, unlike lentiviral-based AD expression, which induces both GABAergic and glutamatergic differentiation. We demonstrate that PB-AD neurons integrate into synaptically connected E/I networks when co-cultured with excitatory NGN2 neurons with synaptic projections proportional to cellular ratios. Using proteomics, patch-clamp electrophysiology, and immunocytochemistry we show that functional synapse maturation correlates with increasing levels of proteins in presynaptic gene sets, resulting in reliable, plastic synapses that synchronously release GABA, whereas postsynaptic function and protein composition are stable over time. We propose that this improved GABAergic induction protocol, which reliably generates pure GABAergic neurons, enables the study of human GABAergic functioning in pure GABAergic networks, in single-neuron (autaptic) cultures, and stable E/I-networks.

Results

GABAergic differentiation of human iPSCs using PiggyBac based delivery of Ascl1 and Dlx2

Overexpression of the transcription factors Ascl1 and Dlx2 drives GABAergic lineage specification of induced pluripotent stem cells (iPSCs) (Yang *et al*., 2017). Previous approaches

103 employed separate lentivectors to express both genes in an inducible manner. We aimed to
104 develop a simplified GABAergic differentiation protocol using a single PiggyBac transposon
105 construct containing both transcription factors (Figure 1A). This vector contains (1) a
106 doxycycline (dox)-inducible expression cassette for *Ascl1* and *Dlx2* from a bidirectional
107 promoter, avoiding variation in expression levels resulting from position effects in multi-
108 cistronic vectors; (2) reverse tetracycline-controlled transactivator (rtTA), required for dox-
109 inducible expression; (3) the puromycin resistance gene (pac), allowing for antibiotic
110 selection, as well as (4) mTagBFP2 (Subach *et al*, 2011), giving transfected cells a fluorescent
111 marker; and (5) Ubiquitous Chromatin Opening Elements (UCOE) (Müller-Kuller *et al*, 2015)
112 and 5'HS chicken β-globin (cHS4) insulator elements (Chung *et al*, 1997). Firstly, we tested
113 whether our newly designed construct could induce GABAergic differentiation (Figure 1B). To
114 this end, we co-transfected this PiggyBac vector with a transposase vector into BIONi010-C
115 iPSCs (Rasmussen *et al*, 2014). After puromycin-selection, all cells expressed mTagBFP2
116 (Figure 1C), confirming successful transgene integration. Upon dox-induction, cells first
117 clustered together (Figure 1D) and after releasing and reseeding at 3 days post-induction
118 (DPI), cells developed a neuronal morphology, which became more distinct within one week
119 (Figure 1E). At 10 weeks post-induction (WPI), neurons displayed MAP2+ dendrites and $VGAT^+$
120 puncta, indicative of GABAergic synapses, whereas glutamatergic $VGLUT1/2^+$ puncta were
121 absent (Figure 1F,G).

122 *GABAergic synaptic transmission in PiggyBac Ascl1/Dlx2 neurons*

123 To confirm the GABAergic identity of PiggyBac-induced neurons we performed voltage-clamp
124 recordings in autaptic cultures (Js *et al*, 2019) between 6 and 10 WPI (Figure 1H). Rapid
125 depolarization to +30 mV induced action potential evoked postsynaptic currents (ePSCs),
126 which displayed slow decay times (τ) characteristic of GABAergic currents (Jones &
127 Westbrook, 1995), as determined by mono-exponential fits (geometric mean (GM) = 104.2 ms,
128 geometric SD factor (GM_{SDf}) = 1.42; Figure 1I,J). Furthermore, virtually all synaptic signalling
129 was abolished after applying the GABA receptor antagonist picrotoxin (PTX), confirming
130 GABAergic synaptic identity (Figure 1I,K).

131 *PiggyBac Ascl1/Dlx2 yields a pure GABAergic neuron population in contrast to lentiviral methods*

132 To benchmark the PiggyBac approach, we compared it with two established lentiviral
133 methods for GABAergic induction (Mossink *et al.*, 2022; Yang *et al.*, 2017) and an NGN2-based
134 protocol for glutamatergic induction (Meijer *et al*, 2019; Schmid *et al.*, 2021) (Figure 1L).
135 Autaptic neurons were generated using all four protocols and ePSC decay time constants
136 were quantified using mono-exponential fits. As expected, NGN2-derived neurons exhibited

137 fast ePSCs decay kinetics typical of glutamatergic transmission (GM = 2.43 ms, GM_{SDf} = 1.39,
138 Figure 1M,N), confirmed pharmacologically and by the presence of VGLUT1/2$^+$ puncta (Figure
139 S1). Surprisingly, decay time constants from neurons generated with the lentiviral GABAergic
140 protocols showed a bimodal distribution which could be fitted with a sum of two gaussians.
141 More than half of the cells in these cultures exhibited ePSC kinetics comparable to those in
142 the NGN2 cultures (Lenti AF: GM = 2.82 ms, GM_{SDf} = 0.58, 72.8% of the fit; Lenti AD: GM = 4.62
143 ms, GM_{SDf} = 0.42, 55.3% of the fit). The remaining cells had more than tenfold larger time
144 constants typical for slow GABAergic ePSCs (Lenti AF: GM = 86.3 ms, GM_{SDf} = 1.56 for 27,2%
145 of the fit; Lenti AD: GM = 60.5 ms, GM_{SDf} = 1.26 for 44.7% of the fit). In contrast, the PB-AD
146 method produced a unimodal population with slowly decaying ePSCs (GM = 78.9 ms, GM_{SDf}
147 = 1.35). Since NGN2 and PB-AD neurons produced decay time constants with unimodal fits,
148 these values were used to determine cut-off thresholds for synaptic identity (glutamatergic:
149 $\tau \leqslant 6$ ms; GABAergic: $\tau \geqslant 30$ ms; mixed: $6 < \tau < 30$ ms). This revealed that 68% of PB-AD
150 neurons exhibited GABAergic currents, while the remaining 32% were synaptically silent
151 (Figure 1O). In contrast, the lentiviral approaches generated a substantial population of
152 glutamatergic (Lenti AF: 43%, Lenti AD: 39%) and mixed (Lenti AF: 9% Lenti AD: 15%)
153 identities. The consistent generation of functional GABAergic neurons and the absence of
154 glutamatergic neurotransmission underscore the reliability of the PB-AD protocol compared
155 to previously described methods.

156 *PiggyBac Ascl1/Dlx2 protocol induces GABAergic neurons across genetic backgrounds*
157 To test for generalizability, we applied the PB-AD protocol to generate neurons from two
158 additional iPSC lines, KOLF2.1J (Pantazis *et al*, 2022) and GM23973 (Nadadhur *et al*, 2019),
159 and characterized their functional properties at 7 and 6 WPI, respectively. In both lines the
160 PB-AD approach produced neurons with GABAergic synaptic projections and slow-decaying
161 synaptic transmission, indicative of GABAergic specification (Figure S2), as was found for the
162 BIONi010-C line. These findings demonstrate the protocol's applicability across genetic
163 backgrounds.

164 *PiggyBac Ascl1/Dlx2 neurons integrate into controlled excitatory/inhibitory networks*
165 To test whether PB-AD neurons integrate into E/I networks alongside glutamatergic neurons,
166 we co-cultured 3 DPI PB-AD neurons with 3 DPI glutamatergic NGN2 neurons in networks
167 containing 100%, 30% (as found in the human cortex (Bakken *et al*, 2021; Fang *et al*, 2022;
168 Loomba *et al*, 2022)) and 0% inhibitory neurons (Figure 2A-C). Immunocytochemistry at 10
169 WPI (Figure 2B,C) revealed comparable neuronal cell densities across all conditions, as
170 measured by NeuN staining, indicating similar viability of PB-AD and NGN2 neurons. (Figure

171 2D). Total dendrite length per field of view increased as the proportion of PB-AD neurons
172 decreased, consistent with the distinct morphological characteristics of GABAergic neurons
173 (Chang *et al*, 2014) (Figure 2E). Pure PB-AD networks contained VGAT$^+$ (GABAergic) synaptic
174 puncta, and NGN2 networks contained VGLUT1/2$^+$ (glutamatergic) synaptic puncta, with in
175 both cases virtually no puncta of the other type present (Figure 2F,G). In contrast, the mixed
176 (30% PB-AD) networks contained both GABAergic and glutamatergic puncta on the same
177 dendrite proportional to cellular ratios, demonstrating that PB-AD neurons are viable
178 components for assembling E/I networks when mixed with NGN2 neurons.

179 *PiggyBac Ascl1/Dlx2 neurons acquire a GABAergic molecular identity over time*

180 Next, we assessed differentiation of PB-AD and NGN2 neurons over time using mass
181 spectrometry-based proteomics. PB-AD co-cultures with rat astrocytes were compared to
182 NGN2 co-cultures at 4, 6, 8, and 10 WPI (Figure 3A). We detected 99,154 human peptide
183 precursors mapping to 7,775 unique proteins across 60 samples that passed quality control.
184 Variability within groups was low-to-moderate with coefficients of variation between 14.6%
185 and 32.2%, reflecting consistent detection across replicates (Figure S3A-B). To remove rat
186 astrocytic signal, subsequent analyses focused on neuronally enriched proteins (1690
187 proteins). Principal component analysis (PCA) on the neuronally-enriched protein
188 abundances (Figure 3B, S3C) revealed clear separation between PB-AD and NGN2 cultures
189 along the first two components (PC1: 71.5% and PC2: 6.1%), as well as the separation of
190 different time points within each culture. More specifically, time points from both PB-AD and
191 NGN2 cultures showed clear separation between 4, 6, and 8 WPI, while cultures at 8 and 10
192 WPI clustered more closely together, suggesting that proteomic maturation plateaus after 8
193 weeks.

194 To assess lineage specification of PB-AD and NGN2 inductions, we annotated cell
195 types based on differentially expressed proteins using cell type specificity scores (CTSS),
196 computed using single-cell RNA expression data from human cortex (Jorstad *et al*, 2023)
197 (Figure S4A). Across all timepoints, canonical GABAergic proteins, including SLC32A1 (VGAT),
198 GAD1, GAD2, were enriched in PB-AD cultures. In addition, other predicted GABAergic
199 proteins, such as CRHBP, FBN2, CRH, and RELN, were enriched in PB-AD neurons. In contrast,
200 only a few predicted glutamatergic proteins (e.g., BDNF, PCP4, CPZ, and ADAMTSL1) were
201 moderately enriched in PB-AD cultures. The glutamatergic marker SLC17A6 (VGLUT2) was
202 enriched in NGN2 cultures, while SLC17A7 (VGLUT1) was not detected (Figure 3C-F).
203 Surprisingly, NGN2 neurons also showed strong enrichment of several proteins typically
204 associated with GABAergic neurons at all timepoints, including SCGN, CALB2, and PVALB.

205 Immunocytochemistry confirmed PVALB expression in the majority of NGN2 neurons (Figure
206 S4B).
207 To quantitatively assess cell type specification, we performed expression-weighted
208 cell type enrichment (EWCE) analysis (Skene & Grant, 2016) on the top 5% upregulated
209 neuronal proteins for each induction for each timepoint. At all timepoints, PB-AD-specific
210 neuronal proteins showed exclusive and significant enrichment for GABAergic neurons, with
211 enrichment levels increasing until 8 WPI (Figure 2G). GABAergic subclass analysis revealed
212 strongest enrichment for VIP$^+$ interneurons from 6-10 WPI (Figure S4C). In contrast, NGN2-
213 specific proteins showed significant enrichment for glutamatergic neurons only at 6 and 10
214 WPI, while also displaying unexpected GABAergic enrichment, reaching significance at 4 and
215 10 WPI (Figure 3H). Subclass enrichment analysis revealed that this unexpected GABAergic
216 enrichment was most likely accounted for by PVALB$^+$ and VIP$^+$ interneuron-like profiles (S4C,
217 S4D). Taken together, PB-AD neurons acquire a stable GABAergic identity over time,
218 characterized by consistent expression of canonical and subtype-specific GABAergic proteins.
219 By contrast, NGN2-induced neurons exhibit a mixed molecular identity, with evidence for
220 partial GABAergic specification in addition to expected glutamatergic features.

221 *Gradual morphological development of PiggyBac Ascl1/Dlx2 neurons*
222 To examine morphological maturation of PB-AD neurons, we performed immunostaining for
223 MAP2, VGAT and VGLUT1/2 in autaptic cultures (Figure 4A). Similar to networks, PB-AD
224 neurons produced only VGAT$^+$ puncta at all timepoints (Figure 4A-C). A progressive increase
225 in dendrite length was observed during maturation (Figure 4D), accompanied by an increase
226 in the total number of VGAT$^+$ puncta per neuron and puncta densities per dendritic length
227 (Figure 4E-F). Additionally, the intensities of VGAT puncta increased over time (Figure 4G),
228 suggesting increased synaptic vesicles per synaptic terminal. Sholl analysis revealed a rise
229 in the number of arborizations during maturation (Figure 4H,I). Interestingly, growth of
230 dendritic length and complexity plateaued by 6 WPI, whereas synaptic projections continued
231 to develop until 8 and 10 WPI. Together, these results demonstrate that PB-AD neurons
232 develop complex neuronal morphologies accompanied by an increase in presynaptic
233 GABAergic terminals during maturation.

234 *Synaptic strengthening during maturation of PiggyBac Ascl1/Dlx2 neurons*
235 Next, we assessed functional maturation in autaptic neurons with voltage-clamp
236 electrophysiology. Firstly, action-potential independent spontaneous release was recorded.
237 Both miniature postsynaptic current (mPSC) frequency and amplitude increased during
238 maturation (Figure 5A-C). Next, neurons were depolarized to induce ePSCs. Across all time

239 points, 70-80% of neurons were synaptically active, producing a charge of at least 1.5 pC
240 within 70 ms after stimulation (Figure 5D). In active cells, both the amplitude and charge of
241 ePSCs increased progressively between 4 and 10 WPI (Figure 5E-G), with the most
242 pronounced change occurring from 8 to 10 WPI. Decay constants remained consistently
243 above 30 ms – characteristic of GABAergic currents (Figure 5H). Interestingly, decay kinetics
244 subtly slowed after 4 WPI, suggesting potential changes in postsynaptic receptor subunits
245 (Dixon *et al*, 2014; Zhang *et al*, 1997).

246 To evaluate the impact of maturation on short-term synaptic plasticity, we applied
247 paired-pulse stimulation at 50 ms, 200 ms, and 1000 ms intervals (Figure 5I-L). This revealed
248 modest synaptic depression which was stable throughout maturation. Only at a 1000 ms
249 interval, synaptic depression increased as neurons matured. Importantly, maturation
250 increased the size of the readily releasable pool (RRP), as determined by back-extrapolation
251 of the charge evoked by 20 Hz stimulus trains, with the biggest change occurring from 8 to
252 10 WPI (Figure 5M-O). Taken together, these findings demonstrate that PB-AD GABAergic
253 neurons develop functional, plastic synapses that strengthen during maturation.

254 *Functional maturation correlates with upregulation of proteins in presynaptic gene sets*

255 To investigate the molecular basis of synaptic maturation, we looked at the differential
256 expression of SYNGO-annotated synaptic proteins between different timepoints of
257 development (4 to 6 WPI, 6 to 8 WPI, and 8 to 10 WPI) (Koopmans *et al*, 2019a) (Figure 6A).
258 Of all 1605 SYNGO-annotated synaptic genes, 929 unique proteins were detected in PB-AD
259 cultures, of which 478 (51%) were differentially expressed in at least one time contrast
260 (Figure 6B, D-F). In NGN2 neurons, 967 unique SYNGO-annotated proteins were identified of
261 which 644 (67%) were differentially expressed in at least one time contrast (Figure 6C, Figure
262 S5A-C). In both cultures, SYNGO-annotated proteins were abundantly regulated between 4
263 and 8 WPI, while only few proteins showed altered expression between 8 and 10 WPI (Figures
264 6B-F, Supplementary table 1). This indicates that proteomic synaptic maturation plateaus
265 after 8 WPI, consistent with what was observed for neuronal-enriched protein expression.

266 To examine specifically how pre- and postsynapses develop over time, we used GOAT
267 (Koopmans, 2024a) to determine which SYNGO gene sets were enriched for developmentally
268 regulated proteins, where the contribution of each protein was weighted by its $\log_2$ (fold
269 change) (Koopmans, 2024a). Strongest enrichment was observed between 4-6 WPI and 6-8
270 WPI, which occurred exclusively in presynaptic gene sets, including *synaptic vesicle* (*SV*),
271 *presynaptic active zone (AZ)*, and *presynaptic membrane* (Figure 6G-L). Between 8-10 WPI only
272 *SV membrane* proteins and its mother term *presynaptic* proteins were enriched. In contrast,

273 no postsynaptic gene sets were significantly enriched in PB-AD cultures, across all time
274 contrasts. To exclude that these results were biased by a few proteins with large effect sizes,
275 additional SYNGO gene set overrepresentation analysis was performed based on the number
276 of upregulated proteins per gene set. This confirmed the exclusive enrichment of presynaptic
277 terms in PB-AD cultures (Figure S5J–L). Upregulated proteins in NGN2 cultures over time
278 similarly showed a preferential enrichment of presynaptic gene sets using GOAT and SYNGO
279 overrepresentation analyses, with no enrichment for postsynaptic gene sets between 6-10
280 WPI. Thus, synaptic strengthening correlates with changes specifically in presynaptic protein
281 levels, while postsynaptic protein levels remain relatively stable over time.

282 In order to test whether our findings on asymmetrical pre- and postsynaptic
283 maturation translate to a more physiological model, we assessed postsynaptic responses to
284 externally applied GABA in E/I networks, as excitation might alter maturation profiles
285 (Paraskevopoulou *et al*, 2019) (Figure 6M). Furthermore, we used gramicidin-perforated patch
286 to allow measurement of postsynaptic responses without influencing the reversal potential
287 for the GABA-receptor (Watanabe & Fukuda, 2015). GABA puffs were applied at varying
288 holding voltages (Figure 6N). The slope of the I/V curve voltages was unaltered by maturation
289 ($p = 0.305$), indicating that the GABAergic postsynaptic response does not change during
290 maturation under these conditions. Thus, increased synaptic strength during synaptic
291 maturation correlates with presynaptic proteomic changes, but not with postsynaptic
292 development also in E/I-networks.

293 *PiggyBac Ascl1/Dlx2 specific synaptic proteins map to cortical interneuron subtypes*

294 Finally, we investigated whether changes in PB-AD and NGN2 SYNGO-annotated proteomes
295 between 4 and 10 WPI are associated with cortical GABAergic and glutamatergic cell types
296 (Jorstad *et al*., 2023) (Figure 7A). PB-AD cultures showed upregulation of predicted GABAergic
297 and medial ganglionic eminence (MGE) and caudal ganglionic eminence (CGE)-specific
298 proteins (Figure 7B). NGN2 cultures showed upregulation of predicted glutamatergic proteins
299 (Figure 7C). Of note, PB-AD and NGN2 cultures showed upregulation of both GABAergic and
300 glutamatergic receptor subunits (Figure S6A,B), although only input of one of the
301 neurotransmitters was present per culture. Canonical subtype markers for both MGE- and
302 CGE-derived subtypes were also detected in PB-AD neurons (S6C,D).

303 To analyze lineage-specific synaptic development in more detail, we next contrasted
304 the developing (WPI 4 to WPI 10) PB-AD and NGN2 SYNGO-annotated proteomes with each
305 other to find proteins that were specifically regulated in each induction. To this end, for each
306 protein we calculated the difference between PB-AD and NGN2 in differential expression

307 between 4-10 WPI (i.e., $\log_2 (FC)_{AD}$- $\log_2 (FC)_{NGN2}$), and selected the 5th and 95th percentile to
308 define induction-specific synaptic proteins (Figure 7A). We then assessed whether these
309 proteins were enriched in either cortical glutamatergic or cortical GABAergic reference
310 expression profiles (Jorstad *et al*., 2023). Overall, this produced lineage-specific enrichments
311 in most gene sets. PB-AD specific synaptic proteins showed the highest GABAergic
312 enrichment in the gene sets *dense core vesicle* (*DCV*), *SV*, *synaptic signalling*, *metabolism* and
313 *presynaptic process* (Figure 7D-E). Conversely, NGN2-specific synaptic proteins that belonged
314 to *synaptic signalling, SV, organization* and *specialization* showed the highest glutamatergic
315 enrichment (Figure 7F-G).
316 As synaptic gene expression profiles have been shown to reflect neuronal subtypes
317 (Roig Adam *et al*, 2023), we queried whether synaptic proteins that specifically increase in
318 PB-AD or NGN2 cultures show enrichment for neuronal (sub)types. In EWCE analysis, the PB-
319 AD-specific synaptic proteins were enriched in GABAergic neurons (Figure 7H), specifically
320 VIP$^+$, SST$^+$, PAX6$^+$ and LAMP5$^+$ interneurons, but not PVALB$^+$ neurons (Figure 7I). NGN2-specific
321 synaptic proteins were enriched in glutamatergic subtypes (IT, L4 IT, L5 ET, L6 CT, and L6b)
322 but also in GABAergic subtypes (Figure 7J), particularly VIP$^+$ interneurons (Figure 7K).
323 Together, these data indicate that PB-AD-based induction leads to GABAergic synaptic
324 specialization with molecular profiles resembling CGE- and MGE-derived interneurons,
325 whereas NGN2 induction leads to induction of neurons that also contain typical GABAergic
326 proteins.
327
328 **Discussion**

329 *Summary*
330 In this work, we present a single-step, transposon-based GABAergic differentiation method,
331 which uses a single vector to overexpress Ascl1/Dlx2, and we provide a detailed
332 characterization of these GABAergic neurons at different developmental timepoints using
333 mass spectrometry proteomics, immunocytochemistry, and patch-clamp electrophysiology.
334 This method is applicable across different genetic backgrounds and produces exclusively
335 GABAergic neurons with a proteomic profile that maps to different cortical interneuron
336 subtypes, particularly VIP+ neurons. Synapses display GABAergic properties such as
337 picrotoxin-sensitive, slowly decaying, evoked postsynaptic currents and short-term
338 depression, similar to primary GABAergic neurons (Ikeda *et al*, 2008; Jiang *et al*, 2000; Lambert
339 & Wilson, 1994; Pearce *et al*, 1995). During development, synapses gradually increase in
340 synaptic strength, which at earlier timepoints correlates with enhanced expression of specific

presynaptic gene sets associated with the active zone, synaptic vesicle, and presynaptic membrane. In contrast, little functional and proteomic changes occur in the postsynapse. Late in development synaptic strength continues to increase, with only minor changes at the proteomic level. PB-AD neurons can be combined with NGN2 neurons to form networks of predefined E/I ratios with corresponding synapse ratios. Taken together, transposon-based GABAergic induction yields pure GABAergic neurons with improved synaptic properties that can be used to build balanced excitation/inhibition networks, for instance for disease modelling in those (many) cases where E/I disbalance has been proposed as a disease mechanism.

PiggyBac Ascl1/Dlx2 neuronal induction produces exclusively GABAergic neurons

By employing autaptic neurons we were able to detect synaptic output on a single neuron scale, which allowed us to accurately quantify lineage specification and demonstrate how pure GABAergic transposon-based induction is compared to lentiviral strategies. Previous studies using a lentiviral approach also detected non-GABAergic currents (Gonzalez-Ramos *et al*, 2021) and reported expression of glutamatergic genes (Barretto *et al*, 2020; Song *et al*, 2021), while others focused on measurements in E/I-networks (Mossink *et al*., 2022; Yang *et al*., 2017) or recorded under conditions that blocked glutamatergic transmission (Marcó de la Cruz *et al*, 2024; Sanchez-Priego *et al*, 2022), making it difficult to compare with our results. As Ascl1 expression, by itself, induces glutamatergic differentiation (Chanda *et al*, 2014; Wu *et al*, 2024), the balance of Ascl1 and Dlx2 expression is likely important in steering differentiation towards a GABAergic fate. The design of our transposon-based induction incorporates multiple features to facilitate this and thereby avoids unwanted glutamatergic specification. Firstly, both factors are present in one cassette and transcribed from a bidirectional promotor. Secondly, a shared integration site could prevent position effects (Gierman *et al*, 2007). Lastly, insulator elements may reduce gene silencing, which is observed for lentiviral cargo (Cabrera *et al*., 2022; Gödecke *et al*, 2017; He *et al*, 2005; Kwak *et al*, 2024; Liew *et al*, 2007; Wolf & Goff, 2009; Yao *et al*., 2004), and less so for transposon delivered transgenes (Ng *et al*., 2021).

Proteomic profiles of PiggyBac Ascl1/Dlx2 neurons map to cortical interneuron subtypes

Cell type enrichment analysis revealed that neuronal proteins that are higher expressed in PB-AD cultures are significantly enriched for GABAergic neurons at all timepoints, with specific enrichment for VIP^+ interneurons from 6 WPI onwards. Zooming in on synaptic proteins that are upregulated specifically in PB-AD cultures between 4-10 WPI showed significant enrichment for all GABAergic interneuron subtypes except $PVALB^+$, suggesting

375 specification towards both MGE- and CGE-derived neurons. In a previous single-cell RNA-
376 sequencing study of lenti-AD induced neurons, predominantly SST^+ neurons were detected
377 at 4 WPI, but later time points were not investigated (Allison *et al*, 2021). Perhaps CGE
378 markers only appear further along the maturation process, or transcriptomics do not
379 accurately recapitulate the molecular identity of these neurons (Lindhout *et al*, 2020; Moritz
380 *et al*, 2019; Titlow *et al*, 2023).

381 NGN2-induction exhibited a mixed glutamatergic and GABAergic molecular identity,
382 although virtually no VGAT puncta were identified and only glutamatergic ePSCs were
383 recorded, consistent with previous reports (Bullmann *et al*, 2024; Fenske *et al*, 2019; Lin *et al*,
384 2021; Meijer *et al*., 2019; Nehme *et al*, 2018; Rhee *et al*, 2019; van Berkel *et al*, 2024). Thus,
385 its proteomic profile does not translate to mixed functional identity, making it a good model
386 for pure glutamatergic neurons.

387 *Enhanced expression of proteins in presynaptic gene sets during synaptic maturation*

388 Our multilevel analysis of GABAergic cultures at different time points between 4 and
389 10 WPI, combining patch-clamp electrophysiology, immunocytochemistry, and mass spec
390 proteomics, revealed the following insights about synapse maturation: Firstly, synaptic
391 strength increased approximately 3-fold during this period. A comparable increase in mPSC
392 frequency and RRP suggests that this is due to an increase in the strength and/or number of
393 presynaptic projections, which is supported by VGAT immunocytochemistry. Similar
394 development has been described for directed-differentiation and safe-harbor AD GABAergic
395 autaptic neurons (Meijer *et al*., 2019; Rhee *et al*., 2019).

396 Secondly, we observed a stark difference between pre- and postsynaptic development.
397 Strong upregulation of *AZ-*, *SV-* and *presynaptic membrane* proteins occurred, while expression
398 changes in proteins in postsynaptic gene sets were minimal. Current responses to GABA puffs
399 remained constant over time, indicating that functional postsynapses already exist at 4 WPI
400 and the expression of GABA receptors remains unaltered at subsequent weeks. This fits with
401 the notion that expression of postsynaptic neurotransmitter receptors precedes presynaptic
402 innervation (Friedman *et al*, 2000; Kwon & Sabatini, 2011; Mammen *et al*, 1997; Petralia,
403 2012; Richards *et al*, 2005). Release from presynaptic projections subsequently induces
404 clustering of postsynaptic molecules, initiating postsynaptic maturation (Andreae & Burrone,
405 2015; Friedman *et al*., 2000; Harms *et al*, 2005; Okabe *et al*, 2001; Sanes & Lichtman, 1999).
406 Indeed, alignment of the pre- and postsynapse and/or clustering of postsynaptic receptors
407 could explain the 1.5-fold increase in mPSC amplitude with the total number of GABA
408 receptors remaining constant. A similar asymmetric proteomic development of the pre- and

postsynapse was observed in NGN2 neurons and has previously also been described for directed differentiation of iPSC-derived neurons (Nadadhur *et al*, 2017; Togo *et al*, 2021).

Thirdly, functional development follows molecular development with a delay. Proteomic changes abruptly stop after 8 WPI, while the number of synapses and synaptic strength continues to increase beyond this point. Possibly, the bulk of *AZ, SV* and *presynaptic membrane* proteins that are upregulated until 8 WPI are needed to create functional presynapses. Enhancement of GABAergic synaptic strength after this timepoint could rely on cell intrinsic and/or astrocyte-induced (Chung *et al*, 2015; Elmariah *et al*, 2004; Liu *et al*, 2022) structural rearrangement, as well as posttranslational modifications of synaptic proteins, which can occur via various mechanisms. For example, posttranslational modification, mediated by e.g. ERK, PKC, PKA, CaMKII and/or RhoA/ROCK signaling, affects many pre- and postsynaptic proteins, including gephyrin (Flores *et al*, 2015; Ghosh *et al*, 2016; Lorenz-Guertin & Jacob, 2018; Tyagarajan *et al*, 2013; Tyagarajan *et al*, 2011), GABA-receptors (Bright & Smart, 2013; Farzana *et al*, 2016; Hao *et al*, 2023; Hausrat *et al*, 2015; Houston *et al*, 2009; Lorenz-Guertin & Jacob, 2018; Lützenkirchen *et al*, 2024; Nakamura *et al*, 2015), SV-anchored synapsins (Cui *et al*, 2008; Song & Augustine, 2023) and microtubules along with their associated proteins (Heisler *et al*, 2011; Jacob *et al*, 2008; Lorenz-Guertin & Jacob, 2018; Prag *et al*, 2007; Velasco *et al*, 2023; Waites *et al*, 2021). These modifications influence the localization and functional properties of these proteins, thereby modulating synaptic strength. Additionally, synaptic strength can be regulated by (trans-synaptic) alignment of functionally related proteins in nanodomains and nanocolumns, enhancing their cooperative interactions (Biederer *et al*, 2017; Olah *et al*, 2023; Sanderson *et al*, 2020; Scimemi & Diamond, 2012; Südhof, 2018, 2021; Tang *et al*, 2016). Of the few proteins that were upregulated – or for the first time detected – in PB-AD neurons at 10 WPI (Table S1), we found several cell adhesion molecules (CAMs) (CNTNAP4, SLITRK1, CDH1, EPHA7, ITGB3, NPTX2, ITGA2, ELFN1, IGSF8 and CNTNAP1) (Beuter *et al*, 2016; Fiederling *et al*, 2011; Karayannis *et al*, 2014; Li *et al*, 2020; Park & Goda, 2016; Ray & Treloar, 2012; Sia *et al*, 2007; Stachniak *et al*, 2019; Um *et al*, 2014; Wiera *et al*, 2022), extra cellular matrix (ECM) proteins (ITGB3, ITGA2, TNC, GPR158 and RELN) (Condomitti *et al*, 2018; Park & Goda, 2016; Quattrocchi *et al*, 2002; Tucić *et al*, 2021; Wiera *et al.*, 2022), and proteins involved in receptor clustering (NPTX2, SLITRK1, PRRT1, ELFN1) (Martin *et al*, 2021; Matsunaga & Aruga, 2021; O'Brien *et al*, 1999; Yim *et al*, 2013). Some of which are known to strengthen GABAergic transmission (Beuter *et al.*, 2016; Karayannis *et al.*, 2014). Altogether, this suggests that maturation and synaptic strengthening in iPSC-derived neuronal synapses depends on

presynaptic development driven by enhanced expression of multiple presynaptic gene sets and alignment/reorganisation of pre- and postsynapse driven by synapse-organising genes.

A versatile in vitro model for studying the role of inhibition in brain disease

Dysfunction of inhibitory neurons and E/I disbalance are common aspect of neurodevelopmental and neurodegenerative disorders (Gabitto *et al*, 2023; Goel *et al*, 2018; Hijazi *et al*, 2020; Malwade *et al*, 2022; Mossner *et al*, 2020; Palop *et al*, 2007b; Zott *et al*, 2018). Given the purity of the GABAergic cultures produced with the PB-AD protocol, neurons generated with this method provide a versatile model to study the role of inhibition and E/I disbalance in these disorders using a human, and patient-own, genetic background. Compared to a safe harbour approach, our method is directly applicable to patient derived iPSCs, which makes it time and cost efficient, and prevents the introduction of clonal gene editing effects. The reliable production of GABAergic autaptic cultures allows for a detailed assessment of interneuron synaptic properties, such as priming, fusion and synaptic plasticity in patient cell lines (Østergaard *et al*, 2025; Öttl *et al*, 2024; van Boven *et al*, 2024). Application to disease-lines will be important steps to substantiate the full potential of this method. To this end, PB-AD neurons can be mixed with NGN2 neurons at defined ratios, enabling accurate modelling of E/I networks at any ratio, including those found in the human brain (Bakken *et al*., 2021; Fang *et al*., 2022; Loomba *et al*., 2022).

Acknowledgements

The authors thank Robbert Zalm and Ingrid Saarloos for their help with cloning and plasmid production, Lisa Laan and Desiree Schut for preparation of glia feeder plates, Judith Huijgen and Solange Lopes Cardozo for preparation and maintenance of iPSCs, and Berna Özer and Remco Klaassen for performing mass-spectrometry proteomics.

This work was supported by the following grants (ZonMW-TOP BECAUSE (91216064), to M.V and L.N.C. ZonMW-PSIDER Brainmodel (10250022110003) to M.V and L.N.C., NWO-Dutch Research Agenda (NWA) NewTDec (1160.18.200) to M.V and L.N.C.), NWO Gravitation program grant BRAINSCAPES (NWO 024.004.012) to M.V. and ZonMW-OPEN (9120232310098) from the Netherlands Organisation for Scientific Research (NWO) to M.V. and L.N.C.

Declaration of interest

The authors declare no competing interests.

477 **Author contributions**

478 M.E.W., and J.M.C.M. designed and produced the PiggyBac construct

479 T.W.v.V, M.A.v.B., K.I.M., R.F.T., A.B.S., R.E.v.K, M.V. and L.N.C. designed the experiments

480 T.W.v.V, M.A.v.B. and J.S. performed and maintained neuronal inductions and cultures

481 T.W.v.V M.A.v.B. performed the patch-clamp experiments with contributions of J.S. to Fig. 1

482 and C.F. to Fig. S2

483 T.W.v.V, M.A.v.B.,. performed the immunocytochemistry experiments with contributions of J.S

484 to Fig. 1

485 K.I.M., and F.K. performed the proteomics experiments and analysis

486 T.W.V.V, M.A.v.B., K.I.M., R.E.v.K, M.V. and L.N.C. designed figures and wrote the manuscript with

487 input from all authors.

488

489 **Methods**

490 **Key resources table**

REAGENT or RESOURCE	SOURCE	IDENTIFIER
Antibodies		
MAP2	Merck Millipore	(Millipore Cat# AB5543, RRID:AB_571049)
VGAT	Synaptic Systems	(Synaptic Systems Cat# 131 002, RRID:AB_887871)
VGLUT1	Antibodies Inc.	(Antibodies Incorporated Cat# 75-066, RRID:AB_2187693)
VGLUT2	Antibodies Inc.	(Antibodies Incorporated Cat# 75-067, RRID:AB_2239153)
NeuN	Merck Millipore	(Millipore Cat# ABN78, RRID:AB_10807945)
Parvalbumin	Synaptic Systems	(Synaptic Systems Cat# 195 004, RRID:AB_2156476)
Bacterial and virus strains		
FUW-TetO-*Ascl1*-T2A-puro	Addgene	RRID:Addgene_973 29

FUW-TetO-*Dlx2* -IRES-hygro	Addgene	RRID:Addgene_97330
FUW-M2rtTA	Addgene	RRID:Addgene_20342
Deposited data		
PRIDE dataset " One-step induction of human GABAergic neurons promotes presynaptic development & synapse maturation"	This study	PXD064163
Transcriptomic cytoarchitecture reveals principles of human neocortex organization	Jorstad, et al. (Jorstad *et al.*, 2023)	RRID:SCR_016152
Experimental models: Cell lines		
BiONI010-C-10	EBiSC	RRID:CVCL_RM84
BioNi010-C-13	EBiSC	RRID:CVCL_RF90
Kolf2.1J	Jackson Laboratory	RRID:CVCL_B5P3
GM23973	Coriell	RRID:CVCL_BW42
Recombinant DNA		
PB-TO-ASCL1-DLX2	This study	RRID:Addgene_182307
Transposase	This study	N/A
Software and algorithms		
DIA-NN 1.8.1	Demichev, et al (2020,2022) (Demichev *et al*, 2020; Demichev *et al*, 2022)	
MS-DAP 1.0.5	Koopmans, et al. 2023 (Koopmans *et al*, 2023)	
DEqMS	Zhu, et al, 2020 (Zhu *et al*, 2020)	
GOAT	Miedema, et al. 2022 (Koopmans, 2024b)	
SynGO	Koopmans, et al. 2019 (Koopmans *et al*, 2019b)	

491

492 *iPSCs origin and culture*

493 Unless stated otherwise, the BiONi010-C-10 stem cell line (EBISC, RRID:CVCL_RM84) was
494 used for all experiments in this study. For glutamatergic induction, a gene-edited variant of
495 the same line containing an integrated NGN2-casette was used (EBISC, RRID:CVCL_RF90). As
496 a genetically independent control the KOLF2.1J (JAX, JiPSC1000, RRID:CVCL_B5P3) and
497 GM23973 (Coriell, RRID:CVCL_BW42) lines were used. All iPSCs were maintained on Matrigel
498 (Cornig) or Geltrex (Fisher Scientific)-coated dishes in Essential 8 (Gibco) or Essential 8 Flex
499 (Gibco) medium and passaged with EDTA and replated in the culture medium supplemented
500 with ROCK inhibitor Y27632 (5 µM, Tetu bio).

501 *Lentiviral infection*

502 Ultrahigh titre lentiviral particles were generated by Alstem (Richmond, CA, USA) from FUW-
503 M2rtTA (Addgene, #20342, RRID:Addgene_20342), FUW-TetO-*Ascl1*-T2A-puro (Addgene
504 #97329, RRID:Addgene_97329), and FUW-TetO-*Dlx2* -IRES-hygro (Addgene #97330,
505 RRID:Addgene_97330). For *Ascl1*+Forskolin, iPSCs were infected with only FUW-M2rtTA and
506 TetO-*Ascl1*-Puro, for *Ascl1* + *Dlx2* induction, iPSCs were infected with all three lentiviruses.
507 For both lentiviral induction methods, 24 hours after dox induction, puromycin (1 µg/ml)
508 selection was performed. For lentiviral *Ascl1* + *Dlx2* induction, additional hygromycin (75
509 µg/ml) selection was performed. For both selection regimes an uninfected control well was
510 included to confirm successful selection before proceeding towards induction.

511 *PiggyBac transfection*

512 To prepare for PiggyBac transfection, iPSCs were released with accutase and plated as single
513 cells on a Matrigel-coated 6-well plate in E8 + ROCK Inhibitor Y27632 at a density of 1500k
514 per well. Cells were placed in the incubator to adhere for 1 to 2 hours. A total of 3 µg of DNA
515 containing the *Ascl1* + *Dlx2* PiggyBac transposon (Presented here; available on Addgene,
516 182307, RRID:Addgene_182307) and transposase constructs (extended data 1) at a 1:3 molar
517 ratio was prepared in 100 µL of opti-MEM (GIBCO, 31985062). To another 100 µL op opti-
518 MEM 5 µL of Lipofectamine STEM (Invitrogen, STEM00001) was added. Opti-MEM
519 preparations were quickly mixed by pipetting, after which the mixture was incubated at RT
520 for 15 to 30 minutes during which cells received fresh E8 + ROCK Inhibitor Y27632 to wash
521 away non-adherent cells. The opti-MEM solution was then added to the cells in a dropwise
522 fashion. 24 hours post transfection, selection with puromycin (1 µg/ml) was initiated to select
523 only for cells containing the transposon, and selection was repeated every 3-4 days.

524 *PB-AD GABAergic neuronal induction*

525 PB-AD positive iPSCs were released with Accutase (Merck) on day post induction (DPI) 0 and
526 replated with at an approximate density of 3.500 cells/cm^2 in N2 medium (DMEM/F12
527 medium, Life technologies) containing Glutamax (200 mM, Life Technologies), dextrose (0.3%,
528 Life Technologies) N2 supplement B (StemCell Technologies), Pen/Strep (0.1%, Gibco), ROCK
529 inhibitor Y27632 (10 µM, Tetubio) and doxycycline hyclate (2 µg/mL) onto Matrigel (Cornig)
530 or Geltrex (Fisher Scientific) coated dishes. On DPI 1, medium was refreshed using the same
531 composition without ROCK inhibitor Y27632. On DPI 2, the medium was refreshed once more
532 with the same composition as on DPI 1, with the addition of 5-Fluoro-2'-deoxyuridine (FUDR)
533 (10 µM, Sigma-Aldrich) or Cytosine β-D-arabinofuranoside (AraC, 20 µM, Sigma-Aldrich) to
534 remove proliferative cells. On DPI 3, neurons were released with accutase, pelleted, and
535 resuspended and plated in Neurobasal medium (Life Technologies) supplemented with
536 Glutamax (200 mM), B27 (0.1%) Pen-Strep (0.1%), fetal bovine serum (0.5%), BDNF (10 ng/ml,
537 Peprotech), CNTF (10ng/ml, Peprotech), GDNF (10 ng/ml, Peprotech) and doxycycline hyclate
538 (2 µg/mL; Sigma-Aldrich). Neurons were plated to the required respective preparations (see
539 *Autaptic culture* and *Network culture*).

540 *Glutamatergic neuronal induction*

541 For glutamatergic induction, Bioni010-C-13 iPSCs were released with Accutase (Merck) on
542 DPI 0 and replated with at an approximate density of 3.500 cells/cm^2 in N2 medium
543 (DMEM/F12 medium, Life technologies) containing Glutamax (200 mM, Life Technologies),
544 dextrose (0.3%, Life Technologies) N2 supplement B (StemCell Technologies), Pen/Strep
545 (0.1%, Gibco) and doxycycline hyclate (2 µg/mL; Sigma-Aldrich) combined with dual-SMAD
546 inhibitors LDN193189 (100 nM, Stemgent), SB431542 (10 µM, Tocris Bioscience), and XAV939
547 (2 µM, Stemgent) NT3 (10 ng/ml, Peprotech) and doxycycline hyclate (2 µg/mL) onto Matrigel
548 (Cornig) or Geltrex (Fisher Scientific) coated dishes. On DPI 1, medium was refreshed using
549 the same composition without ROCK inhibitor Y27632. On DPI 2, the medium was refreshed
550 once more with the same composition as on day 2, with the addition of 5-Fluoro-2'-
551 deoxyuridine (FUDR) (10 µM, Sigma-Aldrich) or Cytosine β-D-arabinofuranoside (AraC, 20 µM,
552 Sigma-Aldrich) to remove proliferative cells. On DPI 3, neurons were released with accutase,
553 pelleted, resuspended and plated in Neurobasal medium (Life Technologies) supplemented
554 with Glutamax (200 mM), B27 (0.1%) Pen-Strep (0.1%), foetal bovine serum (0.5%), BDNF (10
555 ng/ml, Peprotech), CNTF (10ng/ml, Peprotech), GDNF (10 ng/ml, Peprotech) and doxycycline
556 hyclate (2 µg/mL; Sigma-Aldrich). Neurons were plated to the required respective
557 preparations (see *Autaptic culture* and *Network culture*).

558 *Lentiviral GABAergic induction*

559 In general, lentiviral GABAergic induction protocols followed a similar workflow as PB-AD
560 induction. To better adhere to established protocols (Mossink *et al*., 2022; Yang *et al*., 2017),
561 the medium composition differed at certain steps (Figure 1H). For Ascl1 + Forskolin induction,
562 from DPI 0 onwards, Forskolin (10 µM, Merck) was added to the medium up to DPI 14.
563 Furthermore, from DPI0 onwards non-essential amino acids (1:100, Sigma) were added up to
564 day DPI 14. BDNF (10 ng/ml) and NT3 (10 ng/ml) were present from DPI1 onwards. For
565 lentiviral *Ascl1* + *Dlx2* induction BDNF (10 ng/ml) and NT3 (10 ng/ml) were added from DPI
566 0 onward, as well. Furthermore, laminin (1µg/ml, Sigma-Aldrich), cyclic AMP (1 µM, Sigma-
567 Aldrich), and Ascorbic Acid (200 µM, Sigma-Aldrich), were added to the medium at all
568 subsequent refreshments to improve viability.

569 *Autaptic culture*

570 Neurons were plated at a density of ~ 400 cells / cm^2 on micro-islands prepared from rat
571 glial cells plated on agarose-coated coverslips stamped with a custom stamp in Poly-D-
572 Lysine (0.1 mg/ml, Sigma), rat tail collagen (0.7 mg/ml, Corning) and Fibronectin (100 µg/ml,
573 Corning) in acetic acid (10 mM, sigma). Glial islands were prepared approximately 7 days
574 before plating neurons and were treated with AraC (20 µM, Sigma-Aldrich) before plating
575 neurons. Autaptic cultures were refreshed every 7 days with a ~50% media refreshment, with
576 the same medium as used for plating neurons, but omitting doxycycline hyclate (except for
577 Figure 1E-G, where doxycycline hyclate was added up to DPI 14).

578 *Network culture*

579 Neurons were plated at a density of ~ 7000 cells / cm^2 on coverslips covered with a glial-
580 monolayer prepared from rat astrocytes a week in advance and treated with Cytosine β-D-
581 arabinofuranoside (20 µM, Sigma-Aldrich) 24-48 hours before plating neurons. Networks
582 cultures were refreshed with a ~50% media refreshment every 3-4 days, with the same
583 medium as used for plating neurons, but omitting doxycycline hyclate.

584 *Electrophysiology*

585 Whole-cell voltage-clamp recordings ($V_m = -70$ mV) were performed on autaptic neurons,
586 with borosilicate glass pipettes (2 – 5MΩ) filled with (in mM) 136 KCl, 17.8 HEPES, 1 EGTA,
587 0.6 $MgCl_2$, 4 ATP-Mg, 0.3 GTP-Na, 12 phosphocreatine-K_2 and 50 units/mL phosphocreatine
588 kinase (pH = 7.30, 290 mOsmol). The external solution contained in mM: 10 HEPES, 10
589 glucose, 140 NaCl, 2.4 KCl, 4 $MgCl_2$, and 4 $CaCl_2$ (pH = 7.30, 290 mOsmol). Experiments were
590 performed at room temperature (~22°C using a MultiClamp700B amplifier (Axon
591 Instruments) and Digidata 1440A digitizer under control of Clampex 10 software (Molecular

592 devices). Only cells with an access resistance < 15MΩ (80% compensated) and leak current
593 of <300 pA were included. Synaptic responses were elicited by 0.5 ms depolarization to
594 30 mV.
595 For GABA puffs, perforated patch recordings were produced by filling the patch pipette
596 (in mM) 140 KCl, 10 HEPES, gramicidin (100 µg/ml) and allowing cells to perforate for 15-30
597 minutes after reaching a GΩ seal to < 100 MΩ series resistance. Puff pipettes filled with 100
598 µM GABA in ACSF were positioned near the soma, at approximately 25 µm distance. 100 ms
599 puffs were applied at -110, -90, -70, -50, -30 and -10 mV holding voltages to induce GABAergic
600 currents.

601 *Pharmacology*
602 To Block GABA-currents, picrotoxin (100 µM, Hello Bio) was used. A 100 mM stock was
603 prepared in DMSO and was added to the bath to reach the final concentration. To block
604 glutamatergic currents, AP-V (100 µM, R&D systems) and DNQX (40 µM, Tocris) were used.
605 For DNQX, A 1000x of stock of each was prepared in DMSO. For AP-V, the stock was prepared
606 in water.

607 *Analysis electrophysiological data.*
608 Offline analysis was performed using custom-written programs (Huson & Cornelisse, 2019)
609 in Matlab (Mathworks). Experimental conditions were blinded during analysis. In all figures,
610 stimulation artefacts have been removed. For evoked release during 20 Hz stimulation, back-
611 extrapolation of linear fits from the last 20 pulses of the cumulative charge was used to
612 estimate the RRP (y-intercept) (Neher, 2015).

613 *Immunocytochemistry and morphological analysis*
614 Neurons were fixed in ice cold 100% methanol (VWR) for 15 minutes at 4°C, blocked with
615 2.5% normal goat serum (NGS, Life Technologies) and 0.1% Triton X-100 in PBS for
616 45 minutes and incubated with primary antibodies in PBS with 2.5% NGS and 0.1% Triton X-
617 100 overnight at 4°C. The following primary antibodies were used: chicken anti-MAP2
618 (1:1000, Merck AB5543, RRID:AB_571049); rabbit anti-VGAT (1:2000, SySy #131 002,
619 RRID:AB_887871), mouse anti-VGlut1 (1:250, NeuroMab clone N28/9, Antibodies inc. 75-066,
620 RRID:AB_2187693), mouse anti-VGlut2 (1:250, NeuroMab clone N29/29, Antibodies inc. 75-
621 067, RRID:AB_2239153), Rabbit anti-NeuN (1:500, Merck ABN78, RRID:AB_10807945) and
622 anti-Parvalbumin (1:500, SySy #195 004, RRID:AB_2156476). After washing with PBS the next
623 day, cells were incubated for 1 h at room temperature with secondary antibodies
624 conjugated to Alexa dyes (1:1000, Invitrogen Molecular Probes), washed again and mounted

with DABCO-Mowiol (Invitrogen). Images were acquired at 1024x1024 pixels on a Nikon Eclipse Ti confocal laser scanning microscope (40× objective; NA 1.3) with NIS-Elements software. Z-stacks were produced at a 0.5 µm step-size until no more puncta and/or dendrites were in focus. Confocal settings were kept constant for all scans within an experimental week. Analysis of neuronal morphology was performed on maximum-intensity projections using the automated image analysis routine SynD (Schmitz *et al*, 2011) for autaptic neurons and a custom ImageJ workflows for network analysis, in either case, for VGAT and VGLUT puncta counts, only puncta on dendrites were counted.

Statistics of electrophysiological and morphological data

Statistical testing was performed in MATLAB and GraphPad Prism For descriptive statistics (Figure 1) the likelihood of normality vs lognormality was first calculated; for normally distributed data, the arithmetic mean and standard deviation were calculated. For lognormally distributed data, the geometric mean and geometric SD factor were calculated, instead. In autaptic development timelines (Figure 4&5), to test general developmental trajectories, nonparametric Spearman correlations were computed with a two-tailed test for significance and a 95% confidence interval. For timepoint comparisons, Kruskal-Wallis ANOVAs were performed with Dunn's multiple comparisons test. Pairwise comparisons were made between 4 and 6, 6 and 8, and 8 and 10 WPI. #, ##, ###, #### and *ns* represent results of spearman correlation results, *, **, ***, **** and ns represent Kruskal-Wallis ANOVA results. *ns* and ns represent non-significant results. Single, double, triple and quadruple marks represent $p < 0.05$, $p < 0.01$, $p < 0.001$ and $p < 0.0001$, respectively. GABA-puff responses (figure 6O) were fitted using a first-order polynomial linear fit and an extra sum-of-squares F-test was used to determine whether GABA responses were identical throughout development. In plots, unless stated otherwise, the lines in boxplots represent the median value. Crosses represent the mean value. Boxes represent 50% off the values. Circular markers represent individual observations.

Cell pellet harvesting for MS

Cells were washed three times with 1 ml sterile Dulbecco's PBS (Gibco), whereof first twice at 37°C and finally once at 4 °C. Cultures were kept on ice, scraped off using VWR cell lifters, and harvested in 1.5 ml protein LoBind Eppendorf tubes (VWR). Pellets were obtained by centrifugation at 1,000 × g for 5 minutes at 4 °C. Supernatant was removed and pellets were kept at -80 °C before subsequent sample preparation.

MS sample preparation

658 MS sample preparation was performed following the DNA micro spin column suspension
659 trapping protocol (Thanou *et al*, 2023), with some minor adaptations. Cell pellets were
660 extracted and reduced in 6% SDS buffer, containing 50 mM Tris-HCl (pH 8) and 5 mM tris (2-
661 carboxyethyl)phosphine (TCEP), by incubation at 55°C for 15 minutes in a thermomixer set
662 to 1400 RPM. Free sulfhydryl groups were alkylated by incubation with 20 mM methyl
663 methanethiosulfonate (MMTS; 200 mM stock solution) for 15 minutes at RT. Insoluble debris
664 was cleared by centrifugation at 10000g for 1 minute at RT and the supernatant was
665 transferred to a new tube (Eppendorf). Next, samples were acidified by addition of 1.1%
666 phosphoric acid (12% stock solution), mixed with six volumes of binding/washing buffer
667 (90% methanol and 100mM Tris-HCl, pH 8) and loaded onto a plasmid DNA micro column
668 (HiPure from Magen Biotechnology). The protein particulate was retained on the column
669 upon centrifugation at 1400x g for 1 minute and the columns were washed four times with
670 binding/washing buffer. Columns were transferred to a new tube (Eppendorf), supplemented
671 with 500 ng Trypsin/Lys-C (Promega) in 50 mM NH4HCO3 and incubated overnight at 37°C
672 in a humidified incubator. Tryptic peptides were eluted and pooled by subsequent addition
673 of 50 mM NH4HCO3, 0.1% formic acid and 0.1% formic acid in acetonitrile. Collected peptides
674 were dried by SpeedVac and stored at -80°C.

675 *LC-MS Analysis*

676 Each sample of tryptic digest was redissolved in 0.1% formic acid and the peptide
677 concentration was determined by tryptophan-fluorescence assay (Wiśniewski & Gaugaz,
678 2015); 75 ng of peptide was loaded onto an Evotip Pure (Evosep). Peptide samples were
679 separated by standardized 30 samples per day method on the Evosep One liquid
680 chromatography system, using a 15 cm × 150 µm reverse-phase column packed with 1.5 µm
681 C18-beads (EV1137 from Evosep) connected to a 20 µm ID ZDV emitter (Bruker Daltonics).
682 Peptides were electro-sprayed into the timsTOF Pro 2 mass spectrometer (Bruker Daltonics)
683 equipped with CaptiveSpray source and measured with the following settings: Scan range
684 100-1700 m/z, ion mobility 0.65 to 1.5 Vs/cm2, ramp time 100 ms, accumulation time 100
685 ms, and collision energy decreasing linearly with inverse ion mobility from 59 eV at 1.6
686 Vs/cm2 to 20 eV at 0.6 Vs/cm2. Operating in dia-PASEF mode, each cycle took 1.38 s and
687 consisted of 1 MS1 full scan and 12 dia-PASEF scans. Each dia-PASEF scan contained two
688 isolation windows, in total covering 300-1200 m/z and ion mobility 0.65 to 1.50 Vs/cm2. Dia-
689 PASEF window placement was optimized using the py-diAID tool (Skowronek *et al*, 2022). Ion
690 mobility was auto calibrated at the start of each sample (calibrant m/z, 1/K0: 622.029, 0.992
691 Vs/cm2; 922.010, 1.199 Vs/cm2; 1221.991, 1.393 Vs/cm2).

692 *MS data Analysis*

693 DIA-PASEF raw data were processed with DIA-NN 1.8.1 (Demichev *et al*., 2020; Demichev *et*
694 *al*., 2022). An in-silico spectral library was generated from the uniprot human reference
695 proteome (SwissProt and TrEMBL, canonical and additional isoforms, release 2023-2) using
696 Trypsin/P digestion and at most 1 missed cleavage. Fixed modification was set to beta-
697 methylthiolation (C) and variable modifications were oxidation (M) and N-term M excision
698 (at
699 most 1 per peptide). Peptide length was set to 7-30, precursor charge range was set to 2-4,
700 precursor m/z was limited to 280–1220, both MS1 and MS2 mass accuracy were set to 15
701 ppm, scan window was set to 9, double-pass-mode and match-between-runs were enabled.
702 Protein identifiers (isoforms) were used for protein inference. All other settings were left as
703 default.

704 MS-DAP 1.0.5 (Koopmans *et al*., 2023) was used for downstream differential
705 abundance analyses using the DIA-NN results. Filtering and normalization was applied to
706 respective samples per statistical contrast. Peptide-level filtering was configured to retain
707 only peptides identified in at least 4 samples in both experimental conditions (within current
708 contrast) and only proteins with 2 valid peptides were retained. Next, peptide abundance
709 values were normalized by minimizing the mode $\log_2$ (FC) between sample pairs (MWMB
710 algorithm), followed by protein-level mode-between normalization. The DEqMS (Zhu *et al*.,
711 2020) algorithm was used for statistical analysis and resulting p-values were adjusted for
712 multiple testing using the Benjamini–Hochberg False Discovery Rate (FDR) procedure. To
713 investigate proteins with strong differences in detection rates between conditions, e.g.
714 consistently detected in one condition but (near) absent in another, the MS-DAP differential
715 detection test was applied to all proteins that were observed with at least 2 peptides in at
716 least 4 samples in either condition (i.e. confidently detected proteins). Using the default MS-
717 DAP workflow, we merged differential detection (DD) results into the DEqMS result table for
718 the subset of proteins that had both an absolute DD z-score of at least 6 and a smaller
719 adjusted p-value in DD (or no p-value from DEqMS due to a lack of data points in either
720 condition).

721 *Expression-weighted cell type enrichment analysis*

722 Cell type enrichment analysis gives insight into the cell types that potentially drive
723 differential expression. EWCE uses single-cell RNA-sequencing data to generate a probability
724 distribution associated with a gene list having an average level of expression within a cell
725 (Skene & Grant, 2016). Although it's based on RNA expression levels, it can also be applied

726 to proteomics data (Miedema *et al*, 2022). We used published single nucleus RNA-sequencing
727 data (49,495 nuclei) from human cortical brain regions – including middle temporal gyrus,
728 anterior cingulate cortex, primary visual cortex, primary motor cortex, primary somatosensory
729 cortex and primary auditory cortex – published by Jorstad et al (Jorstad *et al.*, 2023). For cell
730 type annotations we used the cell type annotations: class (e.g., GABAergic neurons) and
731 subclass (e.g. SST^+ interneurons) for first and second level EWCE analysis, respectively.
732 Bootstrap enrichment tests were performed using 10,000 reps to look whether gene sets
733 (i.e., foreground) were significantly enriched for a cell class or subclass relative to the
734 background (i.e., all detected proteins included in that contrast). Since we focused on
735 neuronally-enriched proteins or SYNGO-annotated synaptic proteins, we excluded non-
736 neuronal enrichment scores.
737 EWCE calculates cell type-specificity scores (CTSS) for all genes, which is the
738 percentage of mean expression per cell type relative to the sum of the mean expressions of
739 all cell types. We used the CTSS to predict for each protein the cell type the protein probably
740 is derived from. We only included CTSS from genes that passed mRNA detection threshold
741 (mean expression >4 in at least one cell class). Cell type predictions included neuronal
742 (neuronal CTSS > 70%), GABAergic neurons (GABA CTSS > 0.8 and glutamatergic CTSS < 0.1),
743 glutamatergic neurons (glutamatergic CTSS > 0.8 and GABAergic CTSS < 0.1). Cell type
744 predictions were labelled in volcano plots. We also used the EWCE-calculated mean mRNA
745 expression for each cell type to estimate the differential expression of genes in GABAergic
746 vs glutamatergic neurons, which was used in the SYNGO manual colour plots (Figure 6H)).

747 *Heatmaps and line plots*

748 We used the mean log_2-transformed normalized protein intensities per group (i.e., PBAD 4
749 WPI) and plotted these values using line plots in RStudio (Team, 2020) using ggplot
750 (Wickham, 2016). The relative normalized protein intensities (log_2 (FC)) was used in
751 heatmaps, which were produced using Morpheus. To map these proteins to predicted cell
752 types we also show EWCE-calculated cell type specificity scores. All heatmaps visualizations
753 are with fixed colour scaling (i.e., not relative colour scaling per gene), as indicated by
754 heatmap legend.

755 *Gene-set enrichment analysis using GOAT and over-representation analysis using SYNGO*

756 We used the output of the differential abundance analysis using MSDAP (PB-AD 10 vs 4 WPI
757 and NGN2 10 vs 4 WPI) as input for gene-set enrichment analysis using GOAT. The GOAT
758 online v1.0.2 (Koopmans, 2024b) was used to perform gene set enrichment analyses using
759 gene sets from the SynGO knowledgebase v1.2 (Koopmans *et al.*, 2019b). Effect size-derived

760 gene scores (i.e., $\log_2$ (FC)) were used to test for enriched gene sets that contained at least
761 10 and at most 1500 genes (or 50% of the gene list, whichever was smaller) that overlapped
762 with the input gene list. Multiple testing correction was independently applied per gene set
763 "source" (i.e. SYNGO_CC, SYNGO_BP) using Bonferroni adjustment and all p-values were again
764 adjusted using Bonferroni correction to account for 2 separate tests across "sources". The
765 significance threshold for adjusted p-values was set to 0.05. SYNGO over-representation
766 analysis was performed using the same MSDAP output. Foreground was defined as
767 upregulated proteins per contrast (p-adjusted < 0.05 and $\log_2$ (FC) > 0.1), and the background
768 contained all tested genes for that contrast. SynGO release is dataset version: 20231201, and
769 default settings were used. Ontologies are significantly enriched at 1% FDR, while including
770 terms containing at least three matching input genes.

771 *Material availability*
772 PiggyBac *Ascl1-Dlx2* construct is available from Addgene #182307. The mass spectrometry
773 proteomics data have been deposited to the ProteomeXchange Consortium via the PRIDE
774 partner repository (Perez-Riverol *et al*, 2025) with the dataset identifier PXD064163.
775

776 **References**

777 Allison T, Langerman J, Sabri S, Otero-Garcia M, Lund A, Huang J, Wei X, Samarasinghe RA,
778 Polioudakis D, Mody I *et al* (2021) Defining the nature of human pluripotent stem cell-derived
779 interneurons via single-cell analysis. *Stem Cell Reports* 16: 2548-2564

780 Andreae LC, Burrone J (2015) Spontaneous Neurotransmitter Release Shapes Dendritic Arbors
781 via Long-Range Activation of NMDA Receptors. *Cell Rep* 10: 873-882

782 Bakken TE, Jorstad NL, Hu Q, Lake BB, Tian W, Kalmbach BE, Crow M, Hodge RD, Krienen FM,
783 Sorensen SA *et al* (2021) Comparative cellular analysis of motor cortex in human, marmoset
784 and mouse. *Nature* 598: 111-119

785 Barretto N, Zhang H, Powell SK, Fernando MB, Zhang S, Flaherty EK, Ho SM, Slesinger PA,
786 Duan J, Brennand KJ (2020) ASCL1- and DLX2-induced GABAergic neurons from hiPSC-derived
787 NPCs. *J Neurosci Methods* 334: 108548

788 Baum C (2007) Insertional mutagenesis in gene therapy and stem cell biology. *Current opinion*
789 *in hematology* 14: 337-342

790 Beuter S, Ardi Z, Horovitz O, Wuchter J, Keller S, Saha R, Tripathi K, Anunu R, Kehat O, Kriebel
791 M *et al* (2016) Receptor tyrosine kinase EphA7 is required for interneuron connectivity at
792 specific subcellular compartments of granule cells. *Scientific Reports* 6: 29710

793 Biederer T, Kaeser PS, Blanpied TA (2017) Transcellular Nanoalignment of Synaptic Function.
794 *Neuron* 96: 680-696

795 Breschi A, Gingeras TR, Guigó R (2017) Comparative transcriptomics in human and mouse.
796 *Nature Reviews Genetics* 18: 425-440

797 Bright DP, Smart TG (2013) Protein kinase C regulates tonic GABAA receptor-mediated
798 inhibition in the hippocampus and thalamus. *European Journal of Neuroscience* 38: 3408-3423

799 Bullmann T, Kaas T, Ritzau-Jost A, Wöhner A, Kirmann T, Rizalar FS, Holzer M, Nerlich J, Puchkov
800 D, Geis C *et al* (2024) Human iPSC-Derived Neurons with Reliable Synapses and Large
801 Presynaptic Action Potentials. *J Neurosci* 44

802 Busche MA, Eichhoff G, Adelsberger H, Abramowski D, Wiederhold K-H, Haass C, Staufenbiel
803 M, Konnerth A, Garaschuk O (2008) Clusters of Hyperactive Neurons Near Amyloid Plaques
804 in a Mouse Model of Alzheimer's Disease. *Science* 321: 1686-1689

805 Cabrera A, Edelstein HI, Glykofrydis F, Love KS, Palacios S, Tycko J, Zhang M, Lensch S, Shields
806 CE, Livingston M *et al* (2022) The sound of silence: Transgene silencing in mammalian cell
807 engineering. *Cell Systems* 13: 950-973

808 Chanda S, Ang Cheen E, Davila J, Pak C, Mall M, Lee Qian Y, Ahlenius H, Jung Seung W, Südhof
809 Thomas C, Wernig M (2014) Generation of Induced Neuronal Cells by the Single
810 Reprogramming Factor ASCL1. *Stem Cell Reports* 3: 282-296

811 Chang C-L, Trimbuch T, Chao H-T, Jordan J-C, Herman MA, Rosenmund C (2014) Investigation
812 of Synapse Formation and Function in a Glutamatergic-GABAergic Two-Neuron Microcircuit.
813 *The Journal of Neuroscience* 34: 855-868

814 Chung JH, Bell AC, Felsenfeld G (1997) Characterization of the chicken beta-globin insulator.
815 *Proc Natl Acad Sci U S A* 94: 575-580

816 Chung WS, Allen NJ, Eroglu C (2015) Astrocytes Control Synapse Formation, Function, and
817 Elimination. *Cold Spring Harb Perspect Biol* 7: a020370

818 Condomitti G, Wierda KD, Schroeder A, Rubio SE, Vennekens KM, Orlandi C, Martemyanov KA,
819 Gounko NV, Savas JN, de Wit J (2018) An Input-Specific Orphan Receptor GPR158-HSPG
820 Interaction Organizes Hippocampal Mossy Fiber-CA3 Synapses. *Neuron* 100: 201-215.e209

821 Cui Y, Costa RM, Murphy GG, Elgersma Y, Zhu Y, Gutmann DH, Parada LF, Mody I, Silva AJ (2008)
822 Neurofibromin regulation of ERK signaling modulates GABA release and learning. *Cell* 135:
823 549-560

824 Demichev V, Messner CB, Vernardis SI, Lilley KS, Ralser M (2020) DIA-NN: neural networks and
825 interference correction enable deep proteome coverage in high throughput. *Nat Methods* 17:
826 41-44

827 Demichev V, Szyrwiel L, Yu F, Teo GC, Rosenberger G, Niewienda A, Ludwig D, Decker J, Kaspar-
828 Schoenefeld S, Lilley KS *et al* (2022) dia-PASEF data analysis using FragPipe and DIA-NN for
829 deep proteomics of low sample amounts. *Nat Commun* 13: 3944

830 Dixon C, Sah P, Lynch JW, Keramidas A (2014) GABA_A Receptor α and
831 γ Subunits Shape Synaptic Currents via Different Mechanisms *. *Journal of Biological*
832 *Chemistry* 289: 5399-5411

833 Elmariah SB, Hughes EG, Oh EJ, Balice-Gordon RJ (2004) Neurotrophin signaling among
834 neurons and glia during formation of tripartite synapses. *Neuron Glia Biol* 1: 1-11

835 Engle SJ, Blaha L, Kleiman RJ (2018) Best Practices for Translational Disease Modeling Using
836 Human iPSC-Derived Neurons. *Neuron* 100: 783-797

837 Fang R, Xia C, Close JL, Zhang M, He J, Huang Z, Halpern AR, Long B, Miller JA, Lein ES *et al*
838 (2022) Conservation and divergence of cortical cell organization in human and mouse
839 revealed by MERFISH. *Science* 377: 56-62

840 Farzana F, Zalm R, Chen N, Li KW, Grant SG, Smit AB, Toonen RF, Verhage M (2016)
841 Neurobeachin Regulates Glutamate- and GABA-Receptor Targeting to Synapses via Distinct
842 Pathways. *Mol Neurobiol* 53: 2112-2123

843 Fenske P, Grauel MK, Brockmann MM, Dorrn AL, Trimbuch T, Rosenmund C (2019) Autaptic
844 cultures of human induced neurons as a versatile platform for studying synaptic function
845 and neuronal morphology. *Scientific Reports* 9: 4890

846 Fiederling A, Ewert R, Andreyeva A, Jüngling K, Gottmann K (2011) E-cadherin is required at
847 GABAergic synapses in cultured cortical neurons. *Neuroscience Letters* 501: 167-172

848 Flores CE, Nikonenko I, Mendez P, Fritschy JM, Tyagarajan SK, Muller D (2015) Activity-
849 dependent inhibitory synapse remodeling through gephyrin phosphorylation. *Proc Natl Acad*
850 *Sci U S A* 112: E65-72

851 Foss-Feig JH, Adkinson BD, Ji JL, Yang G, Srihari VH, McPartland JC, Krystal JH, Murray JD,
852 Anticevic A (2017) Searching for Cross-Diagnostic Convergence: Neural Mechanisms
853 Governing Excitation and Inhibition Balance in Schizophrenia and Autism Spectrum
854 Disorders. *Biol Psychiatry* 81: 848-861

855 Friedman HV, Bresler T, Garner CC, Ziv NE (2000) Assembly of New Individual Excitatory
856 Synapses: Time Course and Temporal Order of Synaptic Molecule Recruitment. *Neuron* 27:
857 57-69

858 Gabitto MI, Travaglini KJ, Rachleff VM, Kaplan ES, Long B, Ariza J, Ding Y, Mahoney JT, Dee N,
859 Goldy J *et al* (2023) Integrated multimodal cell atlas of Alzheimer's disease. *Res Sq*

860 Gharib WH, Robinson-Rechavi M (2011) When orthologs diverge between human and mouse.
861 *Briefings in Bioinformatics* 12: 436-441

862 Ghosh H, Auguadri L, Battaglia S, Simone Thirouin Z, Zemoura K, Messner S, Acuña MA,
863 Wildner H, Yévenes GE, Dieter A *et al* (2016) Several posttranslational modifications act in
864 concert to regulate gephyrin scaffolding and GABAergic transmission. *Nature Communications*
865 7: 13365

866 Gierman HJ, Indemans MH, Koster J, Goetze S, Seppen J, Geerts D, van Driel R, Versteeg R
867 (2007) Domain-wide regulation of gene expression in the human genome. *Genome Res* 17:
868 1286-1295

869 Gödecke N, Zha L, Spencer S, Behme S, Riemer P, Rehli M, Hauser H, Wirth D (2017) Controlled
870 re-activation of epigenetically silenced Tet promoter-driven transgene expression by
871 targeted demethylation. *Nucleic Acids Research* 45: e147-e147

872 Goel A, Cantu DA, Guilfoyle J, Chaudhari GR, Newadkar A, Todisco B, de Alba D, Kourdougli N,
873 Schmitt LM, Pedapati E *et al* (2018) Impaired perceptual learning in a mouse model of Fragile
874 X syndrome is mediated by parvalbumin neuron dysfunction and is reversible. *Nat Neurosci*
875 21: 1404-1411

876 Gonzalez-Ramos A, Waloschková E, Mikroulis A, Kokaia Z, Bengzon J, Ledri M, Andersson M,
877 Kokaia M (2021) Human stem cell-derived GABAergic neurons functionally integrate into
878 human neuronal networks. *Sci Rep* 11: 22050

879 Hao Y, Liu H, Zeng X-T, Wang Y, Zeng W-X, Qian K-Y, Li L, Chi M-X, Gao S, Hu Z *et al* (2023) UNC-
880 43/CaMKII-triggered anterograde signals recruit GABAARs to mediate inhibitory synaptic
881 transmission and plasticity at C. elegans NMJs. *Nature Communications* 14: 1436

882 Harms KJ, Tovar KR, Craig AM (2005) Synapse-specific regulation of AMPA receptor subunit
883 composition by activity. *J Neurosci* 25: 6379-6388

884 Hausrat TJ, Muhia M, Gerrow K, Thomas P, Hirdes W, Tsukita S, Heisler FF, Herich L, Dubroqua
885 S, Breiden P *et al* (2015) Radixin regulates synaptic GABAA receptor density and is essential
886 for reversal learning and short-term memory. *Nat Commun* 6: 6872

He J, Yang Q, Chang L-J (2005) Dynamic DNA Methylation and Histone Modifications Contribute to Lentiviral Transgene Silencing in Murine Embryonic Carcinoma Cells. *Journal of Virology* 79: 13497-13508

Heisler FF, Loebrich S, Pechmann Y, Maier N, Zivkovic AR, Tokito M, Hausrat TJ, Schweizer M, Bähring R, Holzbaur EL *et al* (2011) Muskelin regulates actin filament- and microtubule-based GABA (A) receptor transport in neurons. *Neuron* 70: 66-81

Hijazi S, Heistek TS, van der Loo R, Mansvelder HD, Smit AB, van Kesteren RE (2020) Hyperexcitable Parvalbumin Interneurons Render Hippocampal Circuitry Vulnerable to Amyloid Beta. *iScience* 23: 101271

Hoffman GE, Schrode N, Flaherty E, Brennand KJ (2019) New considerations for hiPSC-based models of neuropsychiatric disorders. *Molecular Psychiatry* 24: 49-66

Houston CM, He Q, Smart TG (2009) CaMKII phosphorylation of the GABA (A) receptor: receptor subtype- and synapse-specific modulation. *J Physiol* 587: 2115-2125

Huson V, Cornelisse LN, 2019. viewEPSC, 85b8899 ed.

Ikeda K, Yanagawa Y, Bekkers JM (2008) Distinctive Quantal Properties of Neurotransmission at Excitatory and Inhibitory Autapses Revealed Using Variance–Mean Analysis. *The Journal of Neuroscience* 28: 13563-13573

Jacob TC, Moss SJ, Jurd R (2008) GABA (A) receptor trafficking and its role in the dynamic modulation of neuronal inhibition. *Nat Rev Neurosci* 9: 331-343

Jiang L, Sun S, Nedergaard M, Kang J (2000) Paired-pulse modulation at individual GABAergic synapses in rat hippocampus. *J Physiol* 523 Pt 2: 425-439

Jones MV, Westbrook GL (1995) Desensitized states prolong GABAA channel responses to brief agonist pulses. *Neuron* 15: 181-191

Jorstad NL, Close J, Johansen N, Yanny AM, Barkan ER, Travaglini KJ, Bertagnolli D, Campos J, Casper T, Crichton K *et al* (2023) Transcriptomic cytoarchitecture reveals principles of human neocortex organization. *Science* 382

Js, J. RH, Shaib AH, Rehbach K, Lee C, Seif P, Thomas C, Gideons E, Guenther A, Krutenko T *et al* (2019) An Autaptic Culture System for Standardized Analyses of iPSC-Derived Human Neurons. *Cell reports* 27

Karayannis T, Au E, Patel JC, Kruglikov I, Markx S, Delorme R, Héron D, Salomon D, Glessner J, Restituito S *et al* (2014) Cntnap4 differentially contributes to GABAergic and dopaminergic synaptic transmission. *Nature* 511: 236-240

Koopmans F (2024a) GOAT: efficient and robust identification of gene set enrichment. *Communications Biology* 7: 744

Koopmans F (2024b) GOAT: efficient and robust identification of gene set enrichment. *Commun Biol* 7: 744

Koopmans F, Li KW, Klaassen RV, Smit AB (2023) MS-DAP Platform for Downstream Data Analysis of Label-Free Proteomics Uncovers Optimal Workflows in Benchmark Data Sets and Increased Sensitivity in Analysis of Alzheimer's Biomarker Data. *J Proteome Res* 22: 374-386

Koopmans F, Van Nierop P, Andres-Alonso M, Byrnes A, Cijsouw T, Coba MP, Cornelisse LN, Farrell RJ, Goldschmidt HL, Howrigan DP *et al* (2019a) SynGO: An Evidence-Based, Expert-Curated Knowledge Base for the Synapse. *Neuron* 103: 217-234.e214

Koopmans F, van Nierop P, Andres-Alonso M, Byrnes A, Cijsouw T, Coba MP, Cornelisse LN, Farrell RJ, Goldschmidt HL, Howrigan DP *et al* (2019b) SynGO: An Evidence-Based, Expert-Curated Knowledge Base for the Synapse. *Neuron* 103: 217-234.e214

Kwak CS, Oflaz FE, Qiu J, Wang X (2024) Human stem cell-specific epigenetic signatures control transgene expression. *Biochimica et Biophysica Acta (BBA) - Gene Regulatory Mechanisms* 1867: 195063

Kwon HB, Sabatini BL (2011) Glutamate induces de novo growth of functional spines in developing cortex. *Nature* 474: 100-104

Lambert NA, Wilson WA (1994) Temporally distinct mechanisms of use-dependent depression at inhibitory synapses in the rat hippocampus in vitro. *Journal of neurophysiology* 72: 121-130

Li MA, Pettitt SJ, Eckert S, Ning Z, Rice S, Cadiñanos J, Yusa K, Conte N, Bradley A (2013) The piggyBac Transposon Displays Local and Distant Reintegration Preferences and Can Cause Mutations at Noncanonical Integration Sites. *Molecular and Cellular Biology* 33: 1317-1330

Li W, Yang L, Tang C, Liu K, Lu Y, Wang H, Yan K, Qiu Z, Zhou W (2020) Mutations of CNTNAP1 led to defects in neuronal development. *JCI Insight* 5

Liew C-G, Draper JS, Walsh J, Moore H, Andrews PW (2007) Transient and Stable Transgene Expression in Human Embryonic Stem Cells. *Stem Cells* 25: 1521-1528

Lin H-C, He Z, Ebert S, Schörnig M, Santel M, Nikolova MT, Weigert A, Hevers W, Kasri NN, Taverna E *et al* (2021) NGN2 induces diverse neuron types from human pluripotency. *Stem cell reports* 16: 2118-2127

Lindhout FW, Kooistra R, Portegies S, Herstel LJ, Stucchi R, Snoek BL, Altelaar AFM, MacGillavry HD, Wierenga CJ, Hoogenraad CC (2020) Quantitative mapping of transcriptome and proteome dynamics during polarization of human iPSC-derived neurons. *eLife* 9: e58124

Liu J, Feng X, Wang Y, Xia X, Zheng JC (2022) Astrocytes: GABAceptive and GABAergic Cells in the Brain. *Front Cell Neurosci* 16: 892497

Liu Y, Liu H, Sauvey C, Yao L, Zarnowska ED, Zhang S-C (2013) Directed differentiation of forebrain GABA interneurons from human pluripotent stem cells. *Nature protocols* 8: 1670-1679

Lombardo A, Cesana D, Genovese P, Di Stefano B, Provasi E, Colombo DF, Neri M, Magnani Z, Cantore A, Lo Riso P *et al* (2011) Site-specific integration and tailoring of cassette design for sustainable gene transfer. *Nature Methods* 8: 861-869

Loomba S, Straehle J, Gangadharan V, Heike N, Khalifa A, Motta A, Ju N, Sievers M, Gempt J, Meyer HS *et al* (2022) Connectomic comparison of mouse and human cortex. *Science* 377

Lorenz-Guertin JM, Jacob TC (2018) GABA type a receptor trafficking and the architecture of synaptic inhibition. *Developmental Neurobiology* 78: 238-270

Lützenkirchen FP, Zhu Y, Maric HM, Boeck DS, Gromova KV, Kneussel M (2024) Neurobeachin regulates receptor downscaling at GABAergic inhibitory synapses in a protein kinase A-dependent manner. *Commun Biol* 7: 1635

Malwade S, Gasthaus J, Bellardita C, Andelic M, Moric B, Korshunova I, Kiehn O, Vasistha NA, Khodosevich K (2022) Identification of Vulnerable Interneuron Subtypes in 15q13.3 Microdeletion Syndrome Using Single-Cell Transcriptomics. *Biol Psychiatry* 91: 727-739

Mammen AL, Huganir RL, O'Brien RJ (1997) Redistribution and Stabilization of Cell Surface Glutamate Receptors during Synapse Formation. *The Journal of Neuroscience* 17: 7351-7358

Marcó de la Cruz B, Campos J, Molinaro A, Xie X, Jin G, Wei Z, Acuna C, Sterky FH (2024) Liprin-α proteins are master regulators of human presynapse assembly. *Nature Neuroscience* 27: 629-642

Maroof Asif M, Keros S, Tyson Jennifer A, Ying S-W, Ganat Yosif M, Merkle Florian T, Liu B, Goulburn A, Stanley Edouard G, Elefanty Andrew G *et al* (2013) Directed Differentiation and Functional Maturation of Cortical Interneurons from Human Embryonic Stem Cells. *Cell Stem Cell* 12: 559-572

Martin EE, Wleklinski E, Hoang HTM, Ahmad M (2021) Interaction and Subcellular Association of PRRT1/SynDIG4 With AMPA Receptors. *Frontiers in Synaptic Neuroscience* Volume 13 - 2021

981 Matsunaga H, Aruga J (2021) Trans-Synaptic Regulation of Metabotropic Glutamate Receptors
982 by Elfn Proteins in Health and Disease. *Frontiers in Neural Circuits* Volume 15 - 2021

983 Meijer M, Rehbach K, Brunner JW, Classen JA, Lammertse HCA, van Linge LA, Schut D, Krutenko
984 T, Hebisch M, Cornelisse LN *et al* (2019) A Single-Cell Model for Synaptic Transmission and
985 Plasticity in Human iPSC-Derived Neurons. *Cell Rep* 27: 2199-2211 e2196

986 Miedema SSM, Mol MO, Koopmans FTW, Hondius DC, van Nierop P, Menden K, de Veij
987 Mestdagh CF, van Rooij J, Ganz AB, Paliukhovich I *et al* (2022) Distinct cell type-specific
988 protein signatures in GRN and MAPT genetic subtypes of frontotemporal dementia. *Acta*
989 *Neuropathologica Communications* 10: 100

990 Miller JC, Tan S, Qiao G, Barlow KA, Wang J, Xia DF, Meng X, Paschon DE, Leung E, Hinkley SJ
991 *et al* (2011) A TALE nuclease architecture for efficient genome editing. *Nature Biotechnology*
992 29: 143-148

993 Moritz CP, Mühlhaus T, Tenzer S, Schulenborg T, Friauf E (2019) Poor transcript-protein
994 correlation in the brain: negatively correlating gene products reveal neuronal polarity as a
995 potential cause. *Journal of Neurochemistry* 149: 582-604

996 Mossink B, van Rhijn J-R, Wang S, Linda K, Vitale MR, Zöller JEM, van Hugte EJH, Bak J, Verboven
997 AHA, Selten M *et al* (2022) Cadherin-13 is a critical regulator of GABAergic modulation in
998 human stem-cell-derived neuronal networks. *Molecular Psychiatry* 27: 1-18

999 Mossner JM, Batista-Brito R, Pant R, Cardin JA (2020) Developmental loss of MeCP2 from VIP
1000 interneurons impairs cortical function and behavior. *eLife* 9: e55639

1001 Müller-Kuller U, Ackermann M, Kolodziej S, Brendel C, Fritsch J, Lachmann N, Kunkel H, Lausen
1002 J, Schambach A, Moritz T *et al* (2015) A minimal ubiquitous chromatin opening element
1003 (UCOE) effectively prevents silencing of juxtaposed heterologous promoters by epigenetic
1004 remodeling in multipotent and pluripotent stem cells. *Nucleic Acids Res* 43: 1577-1592

1005 Nadadhur AG, Alsaqati M, Gasparotto L, Cornelissen-Steijger P, van Hugte E, Dooves S,
1006 Harwood AJ, Heine VM (2019) Neuron-Glia Interactions Increase Neuronal Phenotypes in
1007 Tuberous Sclerosis Complex Patient iPSC-Derived Models. *Stem Cell Reports* 12: 42-56

1008 Nadadhur AG, Emperador Melero J, Meijer M, Schut D, Jacobs G, Li KW, Hjorth JJJ, Meredith RM,
1009 Toonen RF, Van Kesteren RE *et al* (2017) Multi-level characterization of balanced inhibitory-
1010 excitatory cortical neuron network derived from human pluripotent stem cells. *PLOS ONE* 12:
1011 e0178533

1012 Nakamura Y, Darnieder LM, Deeb TZ, Moss SJ (2015) Regulation of GABAARs by
1013 phosphorylation. *Adv Pharmacol* 72: 97-146

1014 Neher E (2015) Merits and limitations of vesicle pool models in view of heterogeneous
1015 populations of synaptic vesicles. *Neuron* 87: 1131-1142

1016 Nehme R, Zuccaro E, Ghosh SD, Li C, Sherwood JL, Pietilainen O, Barrett LE, Limone F,
1017 Worringer KA, Kommineni S *et al* (2018) Combining NGN2 Programming with Developmental
1018 Patterning Generates Human Excitatory Neurons with NMDAR-Mediated Synaptic
1019 Transmission. *Cell Reports* 23: 2509-2523

1020 Nelson S, Valakh V (2015) Excitatory/Inhibitory Balance and Circuit Homeostasis in Autism
1021 Spectrum Disorders. *Neuron* 87: 684-698

1022 Ng YH, Chanda S, Janas JA, Yang N, Kokubu Y, Südhof TC, Wernig M (2021) Efficient generation
1023 of dopaminergic induced neuronal cells with midbrain characteristics. *Stem Cell Reports* 16:
1024 1763-1776

1025 Nicholas Cory R, Chen J, Tang Y, Southwell Derek G, Chalmers N, Vogt D, Arnold Christine M,
1026 Chen Y-Jiun J, Stanley Edouard G, Elefanty Andrew G *et al* (2013) Functional Maturation of
1027 hPSC-Derived Forebrain Interneurons Requires an Extended Timeline and Mimics Human
1028 Neural Development. *Cell Stem Cell* 12: 573-586

1029 O'Brien RJ, Xu D, Petralia RS, Steward O, Huganir RL, Worley P (1999) Synaptic clustering of
1030 AMPA receptors by the extracellular immediate-early gene product Narp. *Neuron* 23: 309-323

1031 Okabe S, Miwa A, Okado H (2001) Spine formation and correlated assembly of presynaptic
1032 and postsynaptic molecules. *J Neurosci* 21: 6105-6114

1033 Olah SS, Kareemo DJ, Buchta WC, Sinnen BL, Miller CN, Actor-Engel HS, Gookin SE, Winborn
1034 CS, Kleinjan MS, Crosby KC *et al* (2023) Acute reorganization of postsynaptic
1035 GABA_A receptors reveals the functional impact of molecular nanoarchitecture
1036 at inhibitory synapses. *Cell Reports* 42

1037 Østergaard M, Barbagallo P, Frederiksen HRS, Chung WK, Møller RS, Larsen MR, Freude K,
1038 Verhage M, Sørensen JB (2025) SNAP25 variant I67N: synaptic phenotypes, drug response
1039 and proteome changes in human neurons. *Brain*

1040 Öttl M, Toonen RF, Verhage M (2024) Reduced synaptic depression in human neurons carrying
1041 homozygous disease-causing STXBP1 variant L446F. *Hum Mol Genet* 33: 991-1000

1042 Palop JJ, Chin J, Roberson ED, Wang J, Thwin MT, Bien-Ly N, Yoo J, Ho KO, Yu G-Q, Kreitzer A *et*
1043 *al* (2007a) Aberrant Excitatory Neuronal Activity and Compensatory Remodeling of Inhibitory
1044 Hippocampal Circuits in Mouse Models of Alzheimer's Disease. *Neuron* 55: 697-711

1045 Palop JJ, Chin J, Roberson ED, Wang J, Thwin MT, Bien-Ly N, Yoo J, Ho KO, Yu GQ, Kreitzer A *et*
1046 *al* (2007b) Aberrant excitatory neuronal activity and compensatory remodeling of inhibitory
1047 hippocampal circuits in mouse models of Alzheimer's disease. *Neuron* 55: 697-711

1048 Pantazis CB, Yang A, Lara E, McDonough JA, Blauwendraat C, Peng L, Oguro H, Kanaujiya J, Zou
1049 J, Sebesta D *et al* (2022) A reference human induced pluripotent stem cell line for large-scale
1050 collaborative studies. *Cell Stem Cell* 29: 1685-1702.e1622

1051 Paraskevopoulou F, Herman MA, Rosenmund C (2019) Glutamatergic Innervation onto
1052 Striatal Neurons Potentiates GABAergic Synaptic Output. *J Neurosci* 39: 4448-4460

1053 Park YK, Goda Y (2016) Integrins in synapse regulation. *Nature Reviews Neuroscience* 17: 745-
1054 756

1055 Pearce RA, Grunder SD, Faucher LD (1995) Different mechanisms for use-dependent
1056 depression of two GABAA-mediated IPSCs in rat hippocampus. *J Physiol* 484 (Pt 2): 425-435

1057 Peitz M, Krutenko T, Brüstle O (2020) Protocol for the Standardized Generation of Forward
1058 Programmed Cryopreservable Excitatory and Inhibitory Forebrain Neurons. *STAR Protocols* 1:
1059 100038

1060 Perez-Riverol Y, Bandla C, Kundu DJ, Kamatchinathan S, Bai J, Hewapathirana S, John NS,
1061 Prakash A, Walzer M, Wang S *et al* (2025) The PRIDE database at 20 years: 2025 update.
1062 *Nucleic Acids Res* 53: D543-d553

1063 Petralia RS (2012) Distribution of Extrasynaptic NMDA Receptors on Neurons. *The Scientific*
1064 *World Journal* 2012: 267120

1065 Prag S, De Arcangelis A, Georges-Labouesse E, Adams JC (2007) Regulation of post-
1066 translational modifications of muskelin by protein kinase C. *The International Journal of*
1067 *Biochemistry & Cell Biology* 39: 366-378

1068 Quattrocchi CC, Wannenes F, Persico AM, Ciafré SA, D'Arcangelo G, Farace MG, Keller F (2002)
1069 Reelin is a serine protease of the extracellular matrix. *J Biol Chem* 277: 303-309

1070 Rasmussen Mikkel A, Holst B, Tümer Z, Johnsen Mads G, Zhou S, Stummann Tina C, Hyttel P,
1071 Clausen C (2014) Transient p53 Suppression Increases Reprogramming of Human Fibroblasts
1072 without Affecting Apoptosis and DNA Damage. *Stem Cell Reports* 3: 404-413

1073 Ray A, Treloar HB (2012) IgSF8: a developmentally and functionally regulated cell adhesion
1074 molecule in olfactory sensory neuron axons and synapses. *Mol Cell Neurosci* 50: 238-249

1075 Rhee HJ, Shaib AH, Rehbach K, Lee C, Seif P, Thomas C, Gideons E, Guenther A, Krutenko T,
1076 Hebisch M *et al* (2019) An Autaptic Culture System for Standardized Analyses of iPSC-Derived
1077 Human Neurons. *Cell Reports* 27: 2212-2228.e2217

1078 Richards DA, Mateos JM, Hugel S, de Paola V, Caroni P, Gähwiler BH, McKinney RA (2005)
1079 Glutamate induces the rapid formation of spine head protrusions in hippocampal slice
1080 cultures. *Proc Natl Acad Sci U S A* 102: 6166-6171

1081 Roig Adam A, Martínez-López JA, Van Der Spek SJF, Achsel T, Andres-Alonso M, Bagni C, Bayés
1082 À, Biederer T, Brose N, Chua JJE *et al* (2023) Transcriptional diversity in specific synaptic gene
1083 sets discriminates cortical neuronal identity. *Biology Direct* 18

1084 Rubenstein JLR, Merzenich MM (2003) Model of autism: increased ratio of
1085 excitation/inhibition in key neural systems. *Genes, Brain and Behavior* 2: 255-267

1086 Sanchez-Priego C, Hu R, Boshans LL, Lalli M, Janas JA, Williams SE, Dong Z, Yang N (2022)
1087 Mapping cis-regulatory elements in human neurons links psychiatric disease heritability and
1088 activity-regulated transcriptional programs. *Cell Reports* 39: 110877

1089 Sanderson TM, Georgiou J, Collingridge GL (2020) Illuminating Relationships Between the
1090 Pre- and Post-synapse. *Front Neural Circuits* 14: 9

1091 Sanes JR, Lichtman JW (1999) Development of the vertebrate neuromuscular junction. *Annu*
1092 *Rev Neurosci* 22: 389-442

1093 Schmid B, Holst B, Poulsen U, Jørring I, Clausen C, Rasmussen M, Mau-Holzmann UA, Steeg R,
1094 Nuthall H, Ebneth A *et al* (2021) Generation of two gene edited iPSC-lines carrying a DOX-
1095 inducible NGN2 expression cassette with and without GFP in the AAVS1 locus. *Stem Cell*
1096 *Research* 52: 102240

1097 Schmitz SK, Hjorth JJ, Joemai RM, Wijntjes R, Eijgenraam S, de Bruijn P, Georgiou C, de Jong
1098 AP, van Ooyen A, Verhage M (2011) Automated analysis of neuronal morphology, synapse
1099 number and synaptic recruitment. *Journal of neuroscience methods* 195: 185-193

1100 Scimemi A, Diamond JS (2012) The number and organization of Ca2+ channels in the active
1101 zone shapes neurotransmitter release from Schaffer collateral synapses. *J Neurosci* 32:
1102 18157-18176

1103 Sia G-M, Béïque J-C, Rumbaugh G, Cho R, Worley PF, Huganir RL (2007) Interaction of the N-
1104 Terminal Domain of the AMPA Receptor GluR4 Subunit with the Neuronal Pentraxin NP1
1105 Mediates GluR4 Synaptic Recruitment. *Neuron* 55: 87-102

1106 Skene NG, Grant SG (2016) Identification of Vulnerable Cell Types in Major Brain Disorders
1107 Using Single Cell Transcriptomes and Expression Weighted Cell Type Enrichment. *Front*
1108 *Neurosci* 10: 16

1109 Skowronek P, Thielert M, Voytik E, Tanzer MC, Hansen FM, Willems S, Karayel O, Brunner AD,
1110 Meier F, Mann M (2022) Rapid and In-Depth Coverage of the (Phospho-)Proteome With Deep
1111 Libraries and Optimal Window Design for dia-PASEF. *Mol Cell Proteomics* 21: 100279

1112 Sohal VS, Rubenstein JLR (2019) Excitation-inhibition balance as a framework for
1113 investigating mechanisms in neuropsychiatric disorders. *Molecular Psychiatry* 24: 1248-1257

1114 Song S-H, Augustine GJ (2023) Different mechanisms of synapsin-induced vesicle clustering
1115 at inhibitory and excitatory synapses. *Cell Reports* 42

1116 Song S, Ashok A, Williams D, Kaufman M, Duff K, Sproul A (2021) Efficient Derivation of
1117 Excitatory and Inhibitory Neurons from Human Pluripotent Stem Cells Stably Expressing
1118 Direct Reprogramming Factors. *Curr Protoc* 1: e141

1119 Stachniak TJ, Sylwestrak EL, Scheiffele P, Hall BJ, Ghosh A (2019) Elfn1-Induced Constitutive
1120 Activation of mGluR7 Determines Frequency-Dependent Recruitment of Somatostatin
1121 Interneurons. *J Neurosci* 39: 4461-4474

1122 Subach OM, Cranfill PJ, Davidson MW, Verkhusha VV (2011) An enhanced monomeric blue
1123 fluorescent protein with the high chemical stability of the chromophore. *PLoS One* 6: e28674

1124 Südhof TC (2018) Towards an Understanding of Synapse Formation. *Neuron* 100: 276-293

1125 Südhof TC (2021) The cell biology of synapse formation. *J Cell Biol* 220

1126 Tang AH, Chen H, Li TP, Metzbower SR, MacGillavry HD, Blanpied TA (2016) A trans-synaptic
1127 nanocolumn aligns neurotransmitter release to receptors. *Nature* 536: 210-214

1128 Team R, 2020. RStudio: Integrated Development for R. PBC, Boston, MA.

1129 Thanou E, Koopmans F, Pita-Illobre D, Klaassen RV, Özer B, Charalampopoulos I, Smit AB, Li
1130 KW (2023) Suspension TRAPping Filter (sTRAP) Sample Preparation for Quantitative
1131 Proteomics in the Low µg Input Range Using a Plasmid DNA Micro-Spin Column: Analysis of
1132 the Hippocampus from the 5xFAD Alzheimer's Disease Mouse Model. *Cells* 12

1133 Titlow JS, Kiourlappou M, Palanca A, Lee JY, Gala DS, Ennis D, Yu JJS, Young FL, Susano Pinto
1134 DM, Garforth S *et al* (2023) Systematic analysis of YFP traps reveals common mRNA/protein
1135 discordance in neural tissues. *Journal of Cell Biology* 222: e202205129

Togo K, Fukusumi H, Shofuda T, Ohnishi H, Yamazaki H, Hayashi MK, Kawasaki N, Takei N, Nakazawa T, Saito Y *et al* (2021) Postsynaptic structure formation of human iPS cell-derived neurons takes longer than presynaptic formation during neural differentiation in vitro. *Molecular Brain* 14: 149

Tucić M, Stamenković V, Andjus P (2021) The Extracellular Matrix Glycoprotein Tenascin C and Adult Neurogenesis. *Front Cell Dev Biol* 9: 674199

Tyagarajan SK, Ghosh H, Yévenes GE, Imanishi SY, Zeilhofer HU, Gerrits B, Fritschy JM (2013) Extracellular signal-regulated kinase and glycogen synthase kinase 3 β regulate gephyrin postsynaptic aggregation and GABAergic synaptic function in a calpain-dependent mechanism. *J Biol Chem* 288: 9634-9647

Tyagarajan SK, Ghosh H, Yévenes GE, Nikonenko I, Ebeling C, Schwerdel C, Sidler C, Zeilhofer HU, Gerrits B, Muller D *et al* (2011) Regulation of GABAergic synapse formation and plasticity by GSK3beta-dependent phosphorylation of gephyrin. *Proc Natl Acad Sci U S A* 108: 379-384

Um JW, Kim KH, Park BS, Choi Y, Kim D, Kim CY, Kim SJ, Kim M, Ko JS, Lee S-G *et al* (2014) Structural basis for LAR-RPTP/Slitrk complex-mediated synaptic adhesion. *Nature Communications* 5: 5423

van Berkel AA, Lammertse HCA, Öttl M, Koopmans F, Misra-Isrie M, Meijer M, Dilena R, van Hasselt PM, Engelen M, van Haelst M *et al* (2024) Reduced MUNC18-1 Levels, Synaptic Proteome Changes, and Altered Network Activity in STXBP1-Related Disorder Patient Neurons. *Biol Psychiatry Glob Open Sci* 4: 284-298

van Boven MA, Mestroni M, Zwijnenburg PJG, Verhage M, Cornelisse LN (2024) A de novo missense mutation in synaptotagmin-1 associated with neurodevelopmental disorder desynchronizes neurotransmitter release. *Mol Psychiatry* 29: 1798-1809

Velasco CD, Santarella-Mellwig R, Schorb M, Gao L, Thorn-Seshold O, Llobet A (2023) Microtubule depolymerization contributes to spontaneous neurotransmitter release in vitro. *Communications Biology* 6: 488

Waites C, Qu X, Bartolini F (2021) The synaptic life of microtubules. *Curr Opin Neurobiol* 69: 113-123

Watanabe M, Fukuda A (2015) Development and regulation of chloride homeostasis in the central nervous system. *Front Cell Neurosci* 9: 371

Wickham H (2016) *ggplot2: Elegant Graphics for Data Analysis*. Springer International Publishing

Wiera G, Brzdąk P, Lech AM, Lebida K, Jabłońska J, Gmerek P, Mozrzymas JW (2022) Integrins Bidirectionally Regulate the Efficacy of Inhibitory Synaptic Transmission and Control GABAergic Plasticity. *J Neurosci* 42: 5830-5842

Wilber A, Linehan JL, Tian X, Woll PS, Morris JK, Belur LR, McIvor RS, Kaufman DS (2007) Efficient and stable transgene expression in human embryonic stem cells using transposon-mediated gene transfer. *Stem cells* 25: 2919-2927

Wiśniewski JR, Gaugaz FZ (2015) Fast and sensitive total protein and Peptide assays for proteomic analysis. *Anal Chem* 87: 4110-4116

Wolf D, Goff SP (2009) Embryonic stem cells use ZFP809 to silence retroviral DNAs. *Nature* 458: 1201-1204

Wu J, Ren J, Cui H, Xie Y, Tang Y (2024) Rapid and high-purity differentiation of human medium spiny neurons reveals LMNB1 hypofunction and subtype necessity in modeling Huntington's disease. *Inflamm Regen* 44: 7

Yang N, Chanda S, Marro S, Ng Y-H, Janas JA, Haag D, Ang CE, Tang Y, Flores Q, Mall M (2017) Generation of pure GABAergic neurons by transcription factor programming. *Nature methods* 14: 621-628

Yao S, Sukonnik T, Kean T, Bharadwaj RR, Pasceri P, Ellis J (2004) Retrovirus Silencing, Variegation, Extinction, and Memory Are Controlled by a Dynamic Interplay of Multiple Epigenetic Modifications. *Molecular Therapy* 10: 27-36

Yim YS, Kwon Y, Nam J, Yoon HI, Lee K, Kim DG, Kim E, Kim CH, Ko J (2013) Slitrks control excitatory and inhibitory synapse formation with LAR receptor protein tyrosine phosphatases. *Proc Natl Acad Sci U S A* 110: 4057-4062

Zhang SJ, Huguenard JR, Prince DA (1997) GABAA Receptor-Mediated Cl− Currents in Rat Thalamic Reticular and Relay Neurons. *Journal of Neurophysiology* 78: 2280-2286

Zhu Y, Orre LM, Zhou Tran Y, Mermelekas G, Johansson HJ, Malyutina A, Anders S, Lehtiö J (2020) DEqMS: A Method for Accurate Variance Estimation in Differential Protein Expression Analysis. *Mol Cell Proteomics* 19: 1047-1057

Zott B, Busche MA, Sperling RA, Konnerth A (2018) What Happens with the Circuit in Alzheimer's Disease in Mice and Humans? *Annu Rev Neurosci* 41: 277-297

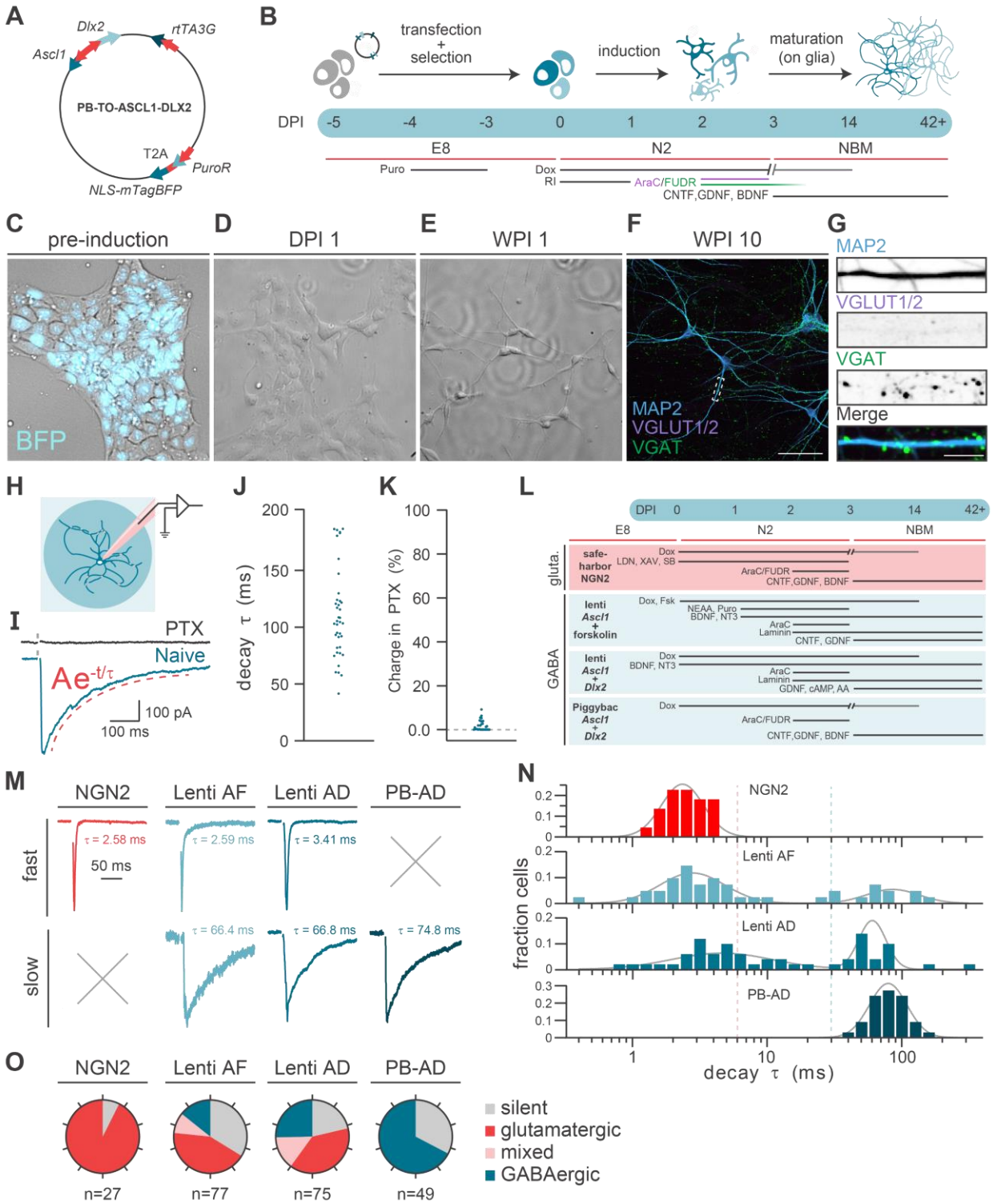

Figure 1. PiggyBac Asc1/Dlx2 efficiently generates pure GABAergic neurons,

A Map of the all-in-one PiggyBac (PB) vector, expressing murine *Ascl1* and *Dlx2* from a bi-directional TRE-responsive promoter, rtTA from the CAG promoter and *pac*-T2A-NLS-mTagBFP from the EF1α promoter. **B** Overview of the protocol for *Ascl1/Dlx2* induction. **C**

Before induction, all iPSCs show nuclear BFP signals, demonstrating successful integration of the PB construct **D** Dox-induced expression of *Dlx2* and *Ascl1* triggers neuronal morphology to arise within one day (DPI1) **E** A week after induction (WPI 1), neural morphology is clearly visible **F** After 10 weeks of culture, PB *Ascl1/Dlx2* induced neurons show mature neuronal morphology with GABAergic synapses (VGAT+ puncta) and no glutamatergic synapses (VGLUT+ puncta) Scale bar: 100 µm **G.** Zoom-in on the dendrite highlighted in F. scale bar = 1 µm. **H** Autaptic cultures of PB *Ascl1/Dlx2* induced neurons were assessed using patch clamp electrophysiology. **I** Evoked postsynaptic currents (PSCs) were fitted using a mono-exponential decay function (red) and their currents were diminished by the application of PTX. **J** Dot-plot of the decay time constants of ePSCs recorded in PB *Ascl1/Dlx2* induced neurons. **K** Dot-plot showing the distribution of cells with 0-10% of the naïve charge remaining in PTX **L** Overview of the four induction methods used, PB *Ascl1/Dlx2* induction was compared to the lentiviral *Ascl1/Dlx2* induction, *Ascl1*+Forskolin induction and *NGN2* glutamatergic induction. **M** Example ePSC traces with either fast or slow decay, as measured in the inductions tested here. **N** Histogram of log-transformed decay time constants (decay τ) measured in neurons induced with the four different induction strategies, together with a 'sum of two gaussians' fit (grey line). **O** Pie-charts showing the percentages of neurons with a slow ($\tau \geqslant 30$ ms), intermediate ($6 > \tau < 30$ ms) and fast ($\tau \leqslant 6$ ms) decay, as well as the percentage of synaptically silent neurons, of neurons generated with the four different induction strategies.

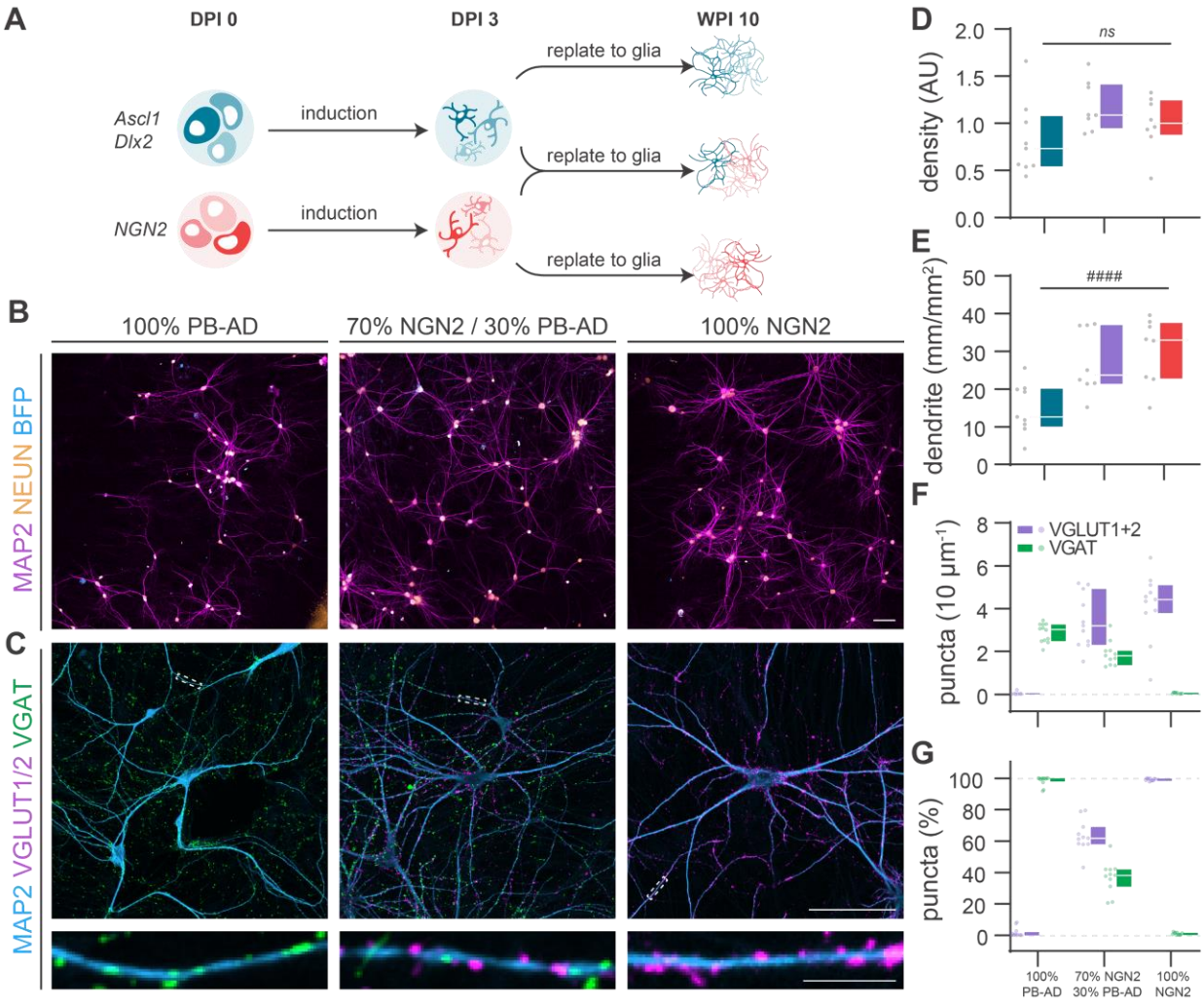

Figure 2. PiggyBac Ascl1/Dlx2 neurons integrate into well-defined excitatory/inhibitory networks upon co-culturing with NGN2 induced neurons

A Schematic of co-culturing protocol in which PiggyBac (PB) Ascl1/Dlx2 (AD) neurons were co-cultured with glutamatergic NGN2 induced neurons to generate excitatory/inhibitory (E/I) co-cultures **B** Representative images of E/I co-cultures at different ratios in which dendrites and neuronal nuclei are visualised using MAP2 and NeuN staining, respectively, and PB-AD neurons visualised by nuclear mTagBFP signals. The E/I-ratio is indicated above each image. Scale bar = 100 µm. **C** Representative images of E/I co-cultures at the same ratios as depicted in (B), stained for MAP2 as dendritic marker and VGAT and VGLUT as markers for GABAergic and glutamatergic synapses, respectively. Scale bars = 100 µm, scale bar zoom in = 10 µm **D** The network density (number of nuclei/field of view) is stable across E/I co-culture ratios. **E** The total dendrite length per field of view decreases as the percentage of plated PB-AD

1239 neurons increases. **F** The density of glutamatergic (VGLUT^{+} puncta) and GABAergic (VGAT^{+})
1240 puncta scales with the percentage of NGN2 and PB-AD neurons plated. **G** Synapse counts
1241 shown in F expressed as the percentage of all synapses counted.
1242

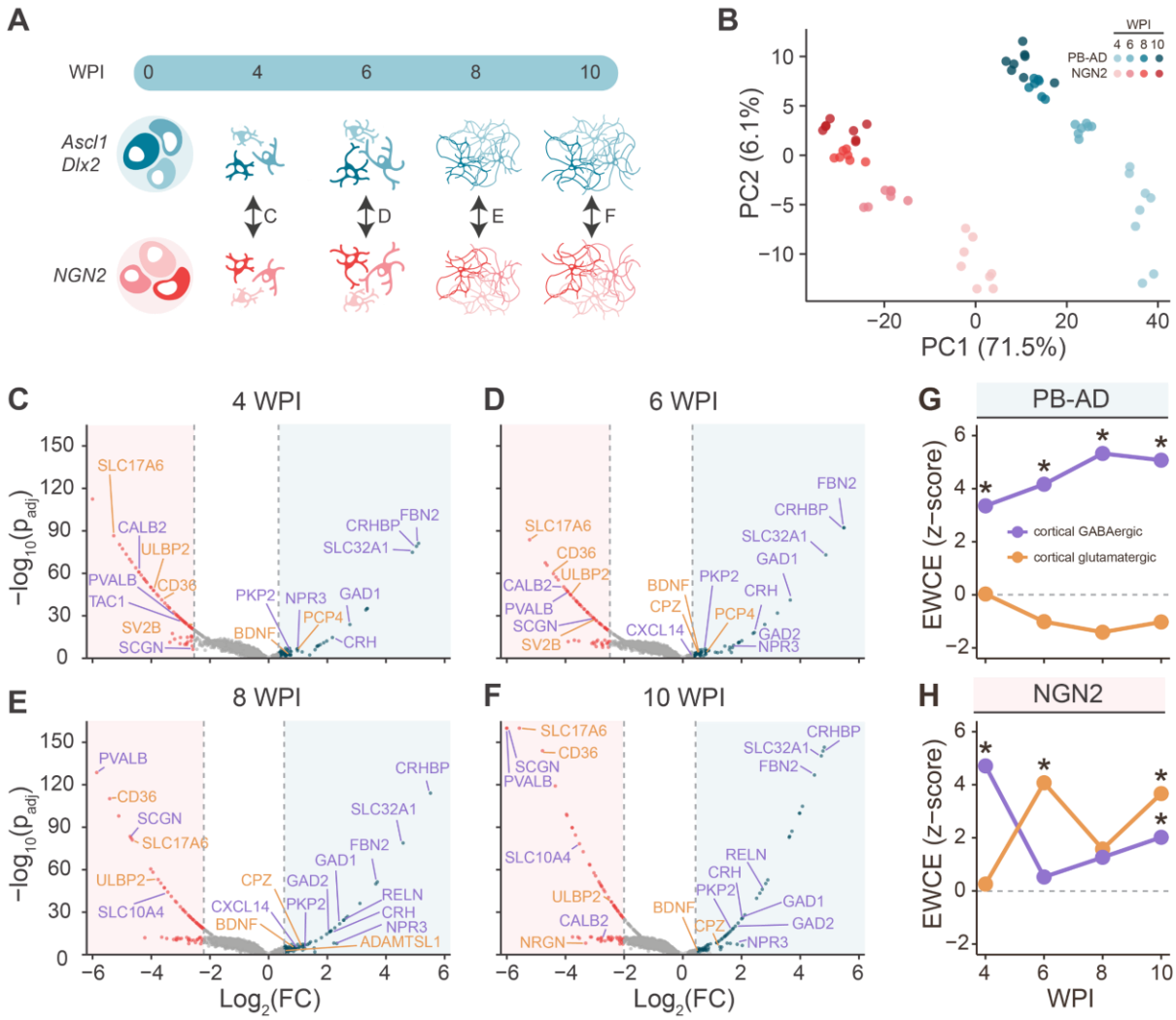

Figure 3. PiggyBac *Ascl1/Dlx2* neurons have a cortical GABAergic proteomic profile.

A. Schematic overview of the proteomics analysis in which PiggyBac (PB) Ascl1/Dlx2 (AD) rat astrocyte co-cultures were compared to NGN2 co-cultures per timepoint. Double-sided arrows indicate the contrasts used for analysis. **B**. PCA analysis on neuronal protein abundances reveals separation of culture types as well as time points along the first two components (PC1: 61.7% and PC2: 8.0%). **C-F**. Volcano plots showing regulation of neuronal proteins in PB-AD cultures and in NGN2 cultures at 4 WPI (**C**), 6 WPI (**D**), 8 WPI (**E**) and 10 WPI (**F**). The top 5% significantly upregulated neuronal proteins in PB-AD are shown as blue dots and those in NGN2 as red dots. Proteins are considered significantly regulated if their adjusted p-value is < 0.05 (significance threshold overlaps with x-axis at this scale and is not shown for clarity of the figure) and their $\log_2$ (FC) lies above the 95th or below the 5th percentile (vertical dashed lines). Label colours indicate the predicted cell types based on

1257 cell type specificity scores (CTSS): regulated GABAergic (purple) and glutamatergic proteins
1258 (orange). Cell type specificity was defined using the following CTSS cutoffs: neuronal proteins
1259 (neuronal CTSS>70%), GABAergic proteins (GABAergic CTSS > 80% and glutamatergic CTSS
1260 < 10%), glutamatergic proteins (glutamatergic CTSS > 80% and GABAergic CTSS < 10%). CTSS
1261 can be found in Figure S6. **G**. EWCE analysis of top 5% upregulated neuronal proteins in PB-
1262 AD cultures reveals specific enrichment for GABAergic neurons, which increased up to 8 WPI.
1263 **H**. EWCE analysis of the top 5% upregulated neuronal proteins in NGN2 cultures reveals
1264 significant enrichment for both glutamatergic and GABAergic neurons depending on the
1265 timepoint.
1266
1267
1268

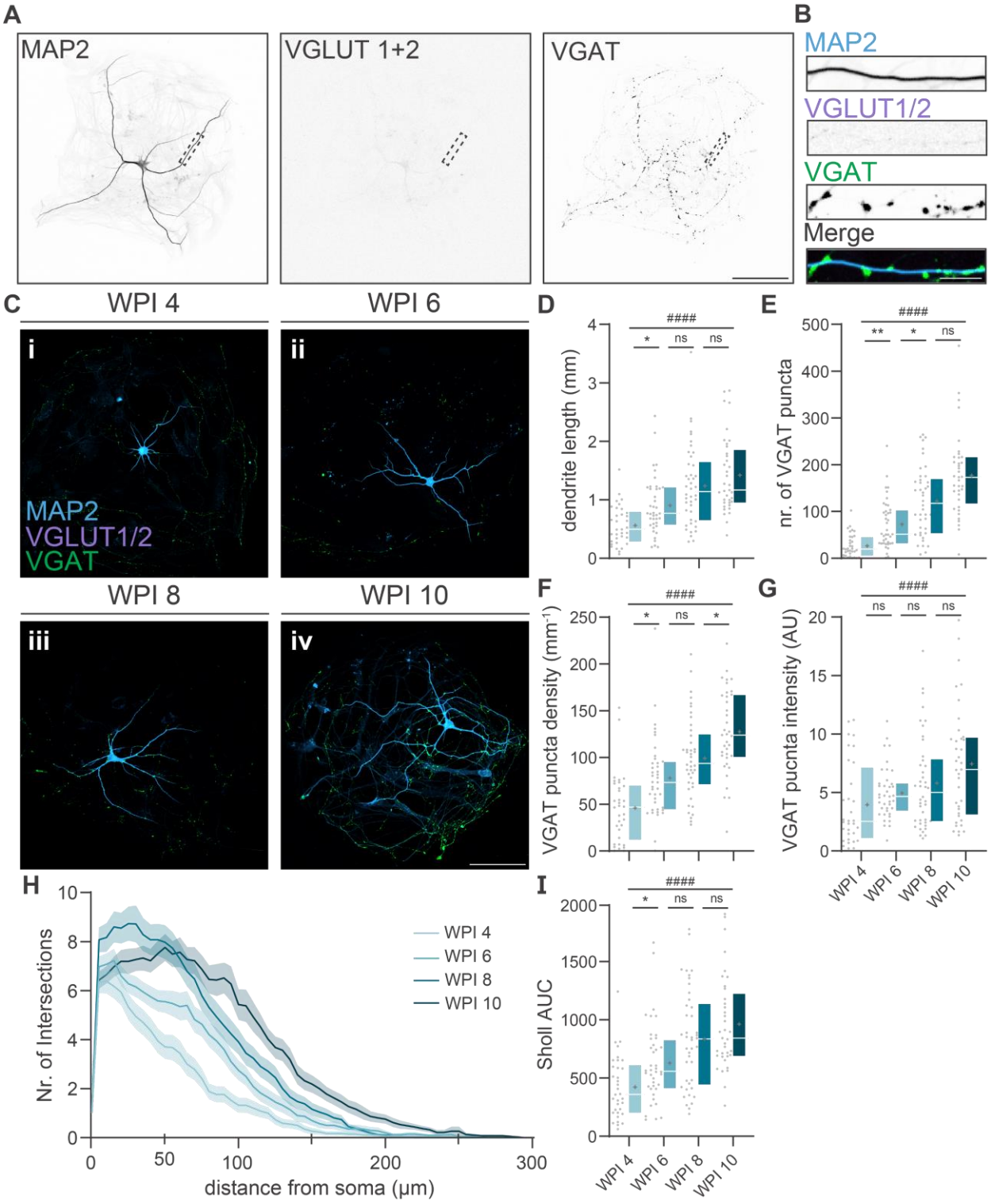

Figure 4. Morphological development of PiggyBac Ascl1/Dlx2 induced neurons

A Representative images of an autaptic PiggyBac (PB) *Ascl1/Dlx2* (AD) induced neuron at week-post-induction 10, stained for MAP2 as dendritic marker, and VGAT and VGLUT1/2 as

GABAergic and glutamatergic markers, respectively. Scale bar: 100 μm **B** Cut-out of dendrite marked in A to illustrate individual synaptic puncta. Scale bar: 10 μm **C** Typical examples of PB-AD autaptic neurons at WPI 4 (i), 6 (ii), 8 (iii) and 10 (iv). Scale bar: 100 μm **D** Total dendrite length quantified. **E** number of GABAergic synapses per neuron. **F** Synaptic density. **G** Average VGAT puncta intensity in arbitrary units (AU). Scale bars: 100 μm. Boxplot whiskers extend the entire data range. **H** Sholl analysis of PB-AD autaptic neurons at WPI 4, 6, 8 and 10. Shaded areas represent the SEM. **I** Quantification of the area under the curve (AUC) of the Sholl histogram shown in (**H**).

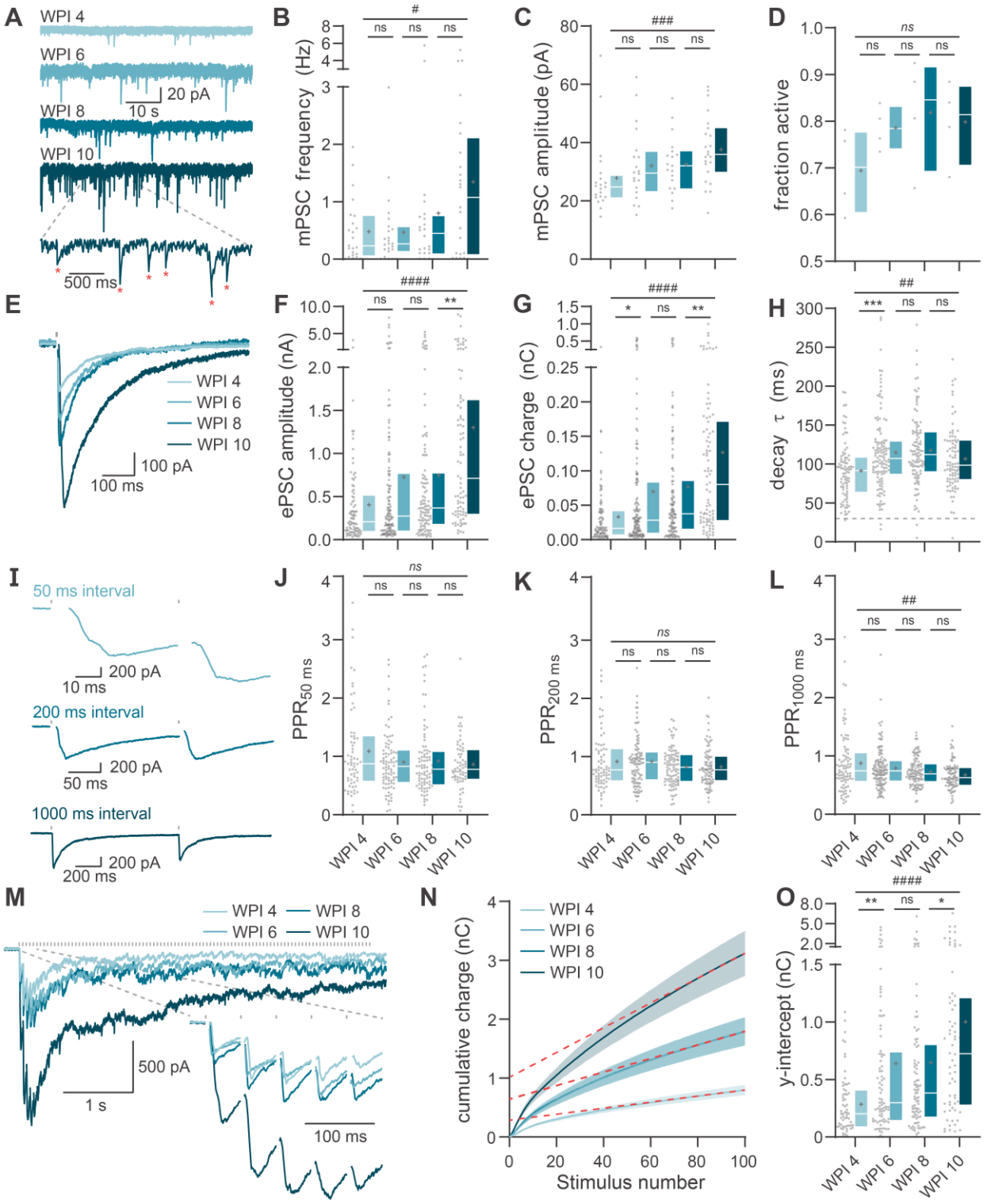

Figure 5. Functional development of PiggyBac Ascl1/Dlx2 induced neurons

A Representative traces of mPSCs recorded from PiggyBac (PB) *Ascl1/Dlx2* (*AD*) neurons (PB-AD) neurons at 4, 6, 8 and 10 weeks post induction (WPI). **B** mPSC frequency and **(C)**

amplitude of PB-AD neurons at 4, 6, 8 and 10 WPI. **D** Boxplots of the average fractions of synaptically active cells at 4, 6, 8 and 10 WPI. Markers represent averages of individual inductions. **E** Representative ePSC traces of at 4, 6, 8 and 10 WPI. **F** Amplitude charge (**G)** and decay time (**H**) constant of ePSCs recorded from PB-AD neurons at 4, 6, 8 and 10 WPI. **I** Representative traces of paired-pulse ePSCs at a 50, 200 and 1000 ms interval at 10 WPI. **J** Quantified paired-pulse amplitude ratios (PPR) at a 50 ms, 200 ms (**K**) and 100 ms (**L**) interval at 4, 6, 8 and 10 WPI. **M** Representative traces of iPSCs evoked by 20Hz stimulus trains from PB-AD neurons at 4, 6, 8 and 10 WPI with zoom in on first five pulses. **N** Plot of cumulative iPSC charge evoked by 20 Hz stimulus trains, with back-extrapolated linear fits displayed in red. Note, WPI 4 and WPI 6 data overlap. **O** RRP estimate obtained from back-extrapolation of linear fits displayed in N.

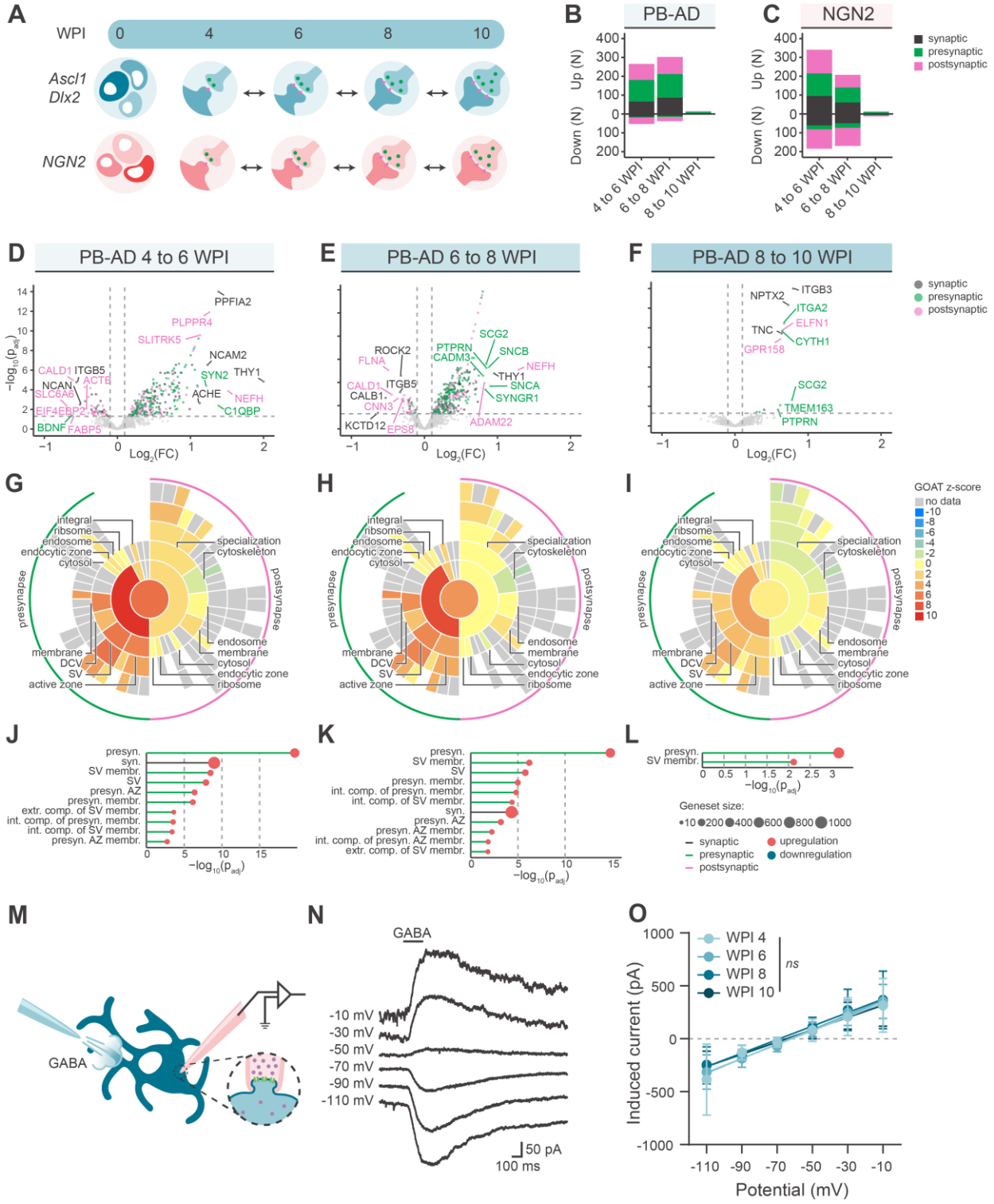

Figure 6. Pre- and postsynaptic maturation of PiggyBac Ascl1/Dlx2 neurons

A. Schematic overview of the proteomics analysis with double-sided arrows indicating the contrasts used for analysis. **B-C**. Stacked bar plots showing the number of up- and

downregulated SYNGO annotated proteins over time, distinguishing synaptic (black), exclusively presynaptic (green) and exclusively postsynaptic (magenta) proteins for PB-AD (**B**) and NGN2 (**C**) neurons. Classifications were assigned based on SynGO annotations, synaptic classification contains both pansynaptic and ambiguously localized synaptic proteins. Regulated proteins have a $\log_2$ (FC) > 0.1, or < -0.1, and adjusted p-value < 0.05. **D-F.** Volcano plots showing regulation of synaptic proteins between 6 and 4 (**D**), 8 and 6 (**E**), and 10 and 8 WPI (**F**). Only SYNGO-annotated proteins are plotted and colour coding refer to significantly regulated synaptic (black) exclusively presynaptic (green) or postsynaptic (pink) annotations. Proteins were regarded significantly regulated when adjusted p-value < 0.05 (dashed horizontal line) and $\log_2$ (FC) > 0.1 or < -0.1 (dashed vertical lines). Top 5% proteins regulated proteins were labelled based on 97.5th and 2.5th percentiles marking genes that drive subsequently detected enrichments. **G-I**. SYNGO plots showing enrichment scores (z-scores) derived from gene-set enrichment analysis with GOAT on SYNGO cellular compartment gene sets, using differential expression output of 6 vs 4 (G), 8 vs 6 (H) and 10 vs 8 WPI (I),. Negative z-scores reflect enrichments primarily driven by downregulated proteins and vice versa for positive z-scores. **J-L.** Lollipop charts showing significant ontologies with their corresponding adjusted p-values and the number of genes part of the gene set as analysed by GOAT for 6 vs 4 (J), 8 vs 6 (K) and 8 vs 10 WPI (L) **M.** Schematic overview of the GABA puff experiment, in which perforated-patch was performed on PB-AD neurons in E/I-networks and GABA was applied to measure the postsynaptic current it produced. **N.** Typical example of the postsynaptic current produced by GABA puff at different holding voltages. **O.** Linear fit of PSC amplitudes as measured in response to GABA puff at 4, 6, 8 and 10 WPI. Error bars represent the SD.

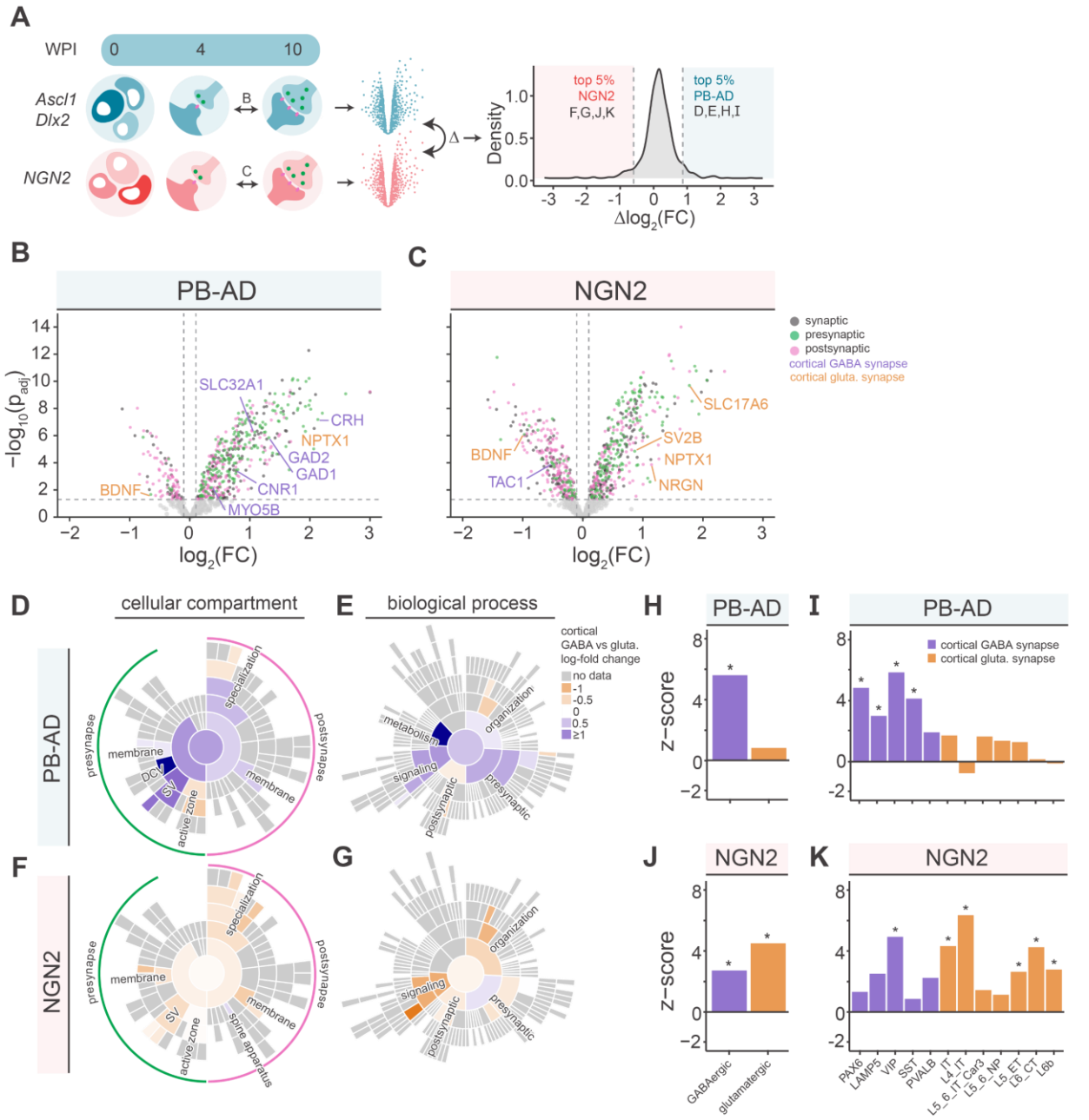

Figure 7. Specialization of PiggyBac Ascl1/Dlx2 and NGN2 neurons into cortical subtypes

A. Schematic overview of the proteomics analysis pipeline. The differential expression of synaptic proteins over time (10 vs 4 WPI) was first quantified for PB-AD and NGN2 culture separately. The difference in expression over time between PB-AD and NGN2 (delta- $\log_2$ (FC)) was next calculated, enabling identification of proteins with PB-AD- or NGN2-specific temporal profiles. Density plot showing 5th and 95th percentiles (dashed vertical lines) selections of proteins that have strong differential temporal regulation (i.e., high or low

delta- log_2 (FC)) in PB-AD compared to NGN2, and vice versa. **B-C**. Volcano plots showing regulation of synaptic proteins between 10 and 4 WPI. Proteins are considered regulated when the log_2 (FC) > 0.1 or < -0.1 (dashed vertical lines) and adjusted p-value < 0.05 (dashed horizontal line). Only SYNGO-annotated proteins are plotted, and dot colors refer to significantly regulated synaptic (black) exclusively presynaptic (green) or postsynaptic (pink) annotations. Label colours indicate for predicted cortical GABAergic- (purple) or glutamatergic (orange) regulated proteins. **D-G** SYNGO sunburst plots showing the GABAergic and glutamatergic specification of PB-AD and NGN cultures. The SYNGO sunburst inputs are the proteins that are part of the 5th (**F-G**) and 95th percentiles (**D-E**) from the delta-log_2 (FC) distribution (**A**), which represent the top 5% exclusively PB-AD and NGN2 regulated proteins, respectively. GABAergic or glutamatergic annotation for these SYNGO terms is estimated based on the differential RNA expression (log_2 (FC)) between cortical GABAergic and glutamatergic neurons of corresponding genes (Jorstad *et al.*, 2023). Both cellular compartment (**D-F**) and biological process (**E-G**) gene sets were used. **H-K**. EWCE analysis of PB-AD-specific (**H-I**) or NGN2-specific proteins (**J-K**) show enrichment for GABAergic and glutamatergic cell sub (classes), respectively. IT and ET refer to intra- and extratelenchephalic-projecting neurons and NP refers to near-projecting neurons (Jorstad *et al.*, 2023).

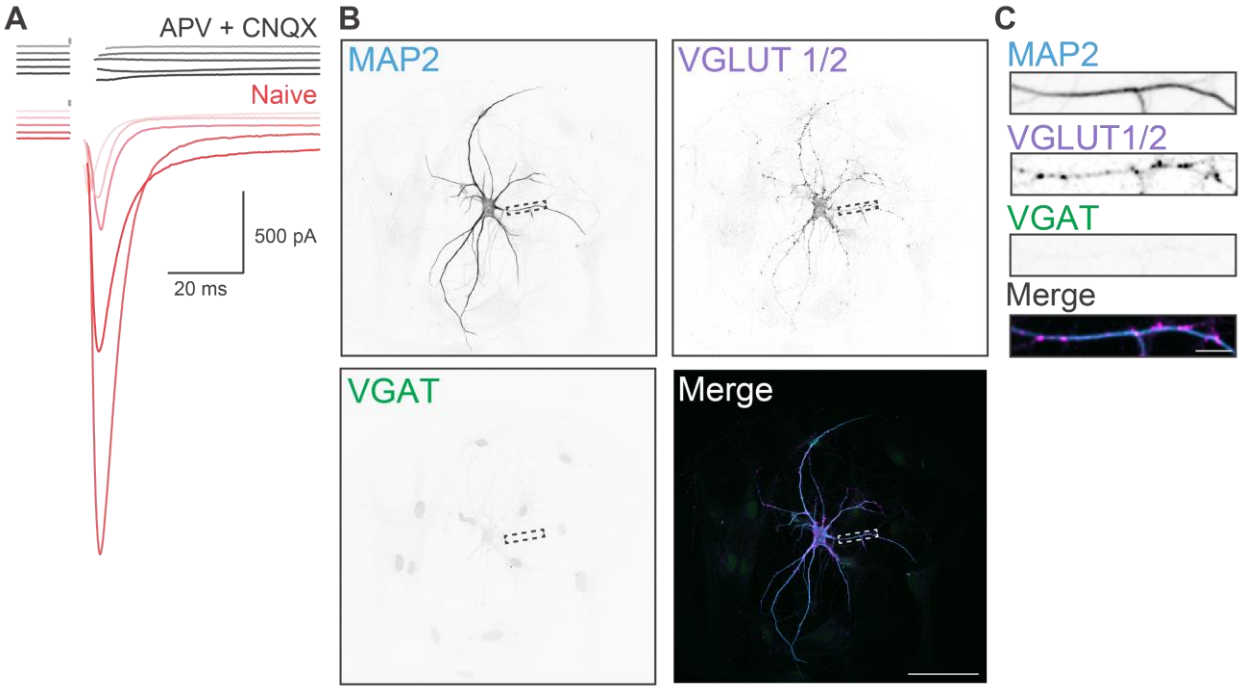

Figure S1. NGN2 neurons produce glutamatergic transmission

A Voltage clamp recordings of 6 WPI NGN2 autaptic neurons after stimulation, in normal ACSF (Naive) and in presence of glutamatergic receptor blockers (APV + CNQX). Synaptic transmission was fully abolished by blockers, illustrating that NGN2 neurons are glutamatergic. **B-C** Examples of immunocytochemistry for MAP2, VGAT and VGLUT1+2 performed on NGN2 autaptic neurons, with zoom in on a length of dendrite (**C**). Scale bar = 100 µm, zoom in scale bar = 10 µm

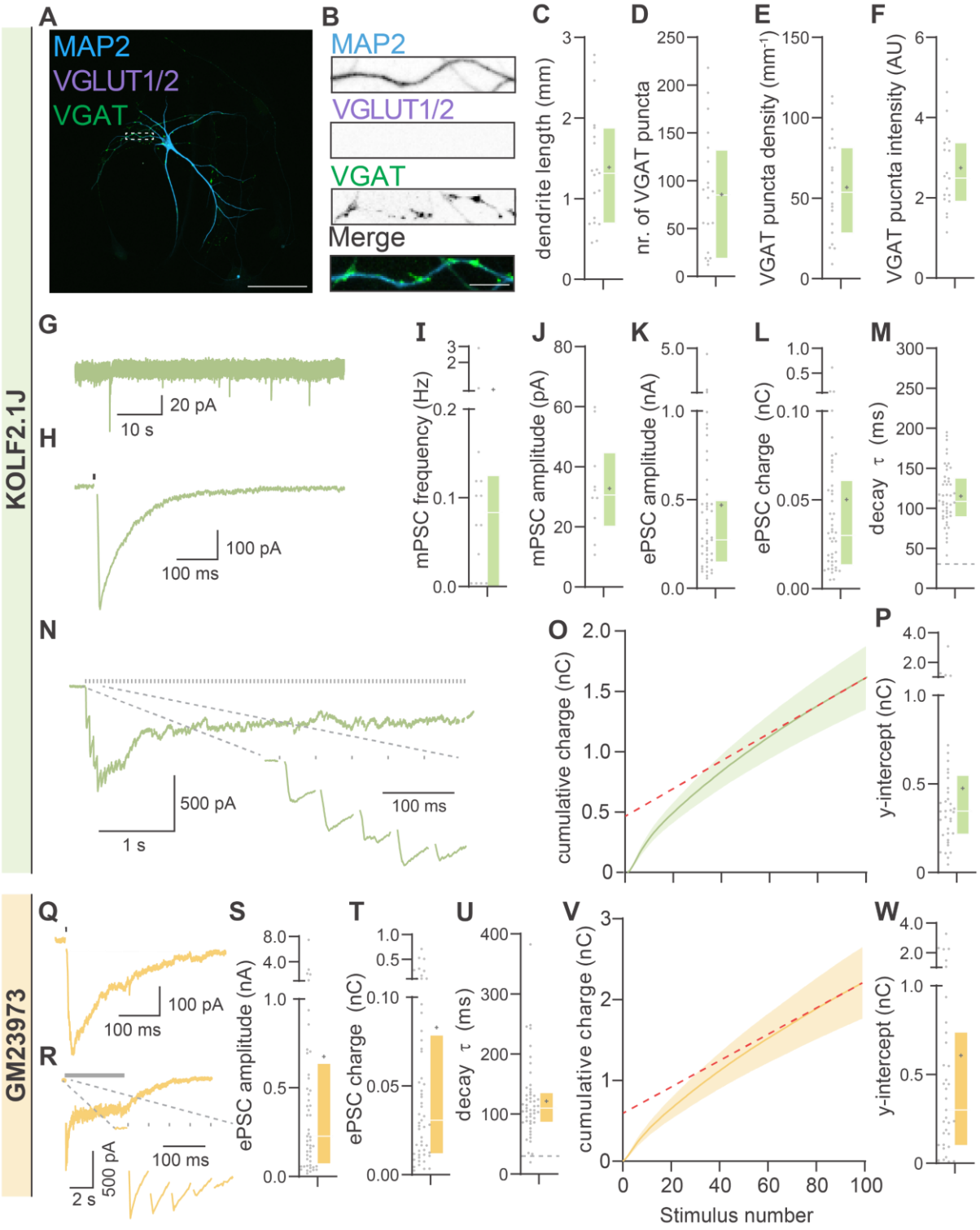
KOLF2.1J
GM23973
A
MAP2
VGLUT1/2
VGAT
B
MAP2
VGLUT1/2
VGAT
Merge
C
dendrite length (mm)
D
nr. of VGAT puncta
E
VGAT puncta density (mm⁻¹)
F
VGAT pucnta intensity (AU)
G
20 pA
10 s
H
100 pA
100 ms
I
mPSC frequency (Hz)
J
mPSC amplitude (pA)
K
ePSC amplitude (nA)
L
ePSC charge (nC)
M
decay τ (ms)
N
500 pA
1 s
100 ms
O
cumulative charge (nC)
P
y-intercept (nC)
Q
100 pA
100 ms
R
500 pA
2 s
100 ms
S
ePSC amplitude (nA)
T
ePSC charge (nC)
U
decay τ (ms)
V
cumulative charge (nC)
Stimulus number
W
y-intercept (nC)

Figure S2. PiggyBac Ascl1/Dlx2 induction reliably generates GABAergic neurons in the KOLF2.1J and GM23973 line

A Representative images of PiggyBac (PB) Ascl1/Dlx2 (AD) neurons induced from KOLF1.2J iPSCs at 7 weeks post induction (WPI), stained for MAP2 as dendritic marker, and VGAT and VGLUT1/2 as GABAergic and glutamatergic markers, respectively**.** Scale bar: 100 µm **B** Zoom-in on dendrite to illustrate punctate VGAT staining. Scale bar: 10 µm **C.** Total dendrite length and (**D**) number of GABAergic synapses per neuron. **E** Synaptic density and intensity (**F**). **G** Representative mPSC trace and (**H**) representative ePSC trace from PB-AD neurons induced from the KOLF2.1J line. **I** Frequency and (**J**) amplitude of miPSCs. **K** Amplitude, (**L**) charge and (**M**) decay time constant of iPSCs in PB-AD neurons generated from the KOLF2.1J line. **N** Representative trace of iPSCs evoked by 20Hz stimulation trains with zoom-in on first five pulses in KOLF2.1J. **O** Plot of cumulative iPSC amplitudes evoked by 20 Hz stimulus trains, with back-extrapolated linear fits displayed in red. **P** RRP estimate obtained from back-extrapolation of linear fits displayed in (**M**). **Q**. representative ePSC traces from PB-AD neurons induced from the GM23973 line. **R.** Representative trace of iPSCs evoked by 20Hz stimulation trains with zoom-in on first five pulses in GM23973. **S** Amplitude, (**T**) charge and (**U**) decay time constant of iPSCs in PB-AD neurons generated from the GM23973.1J line. **V** Plot of cumulative iPSC amplitudes evoked by 20 Hz stimulus trains, with back-extrapolated linear fits displayed in red. **W** RRP estimate obtained from back-extrapolation of linear fits displayed in (M). Boxplot whiskers extend the entire data range.

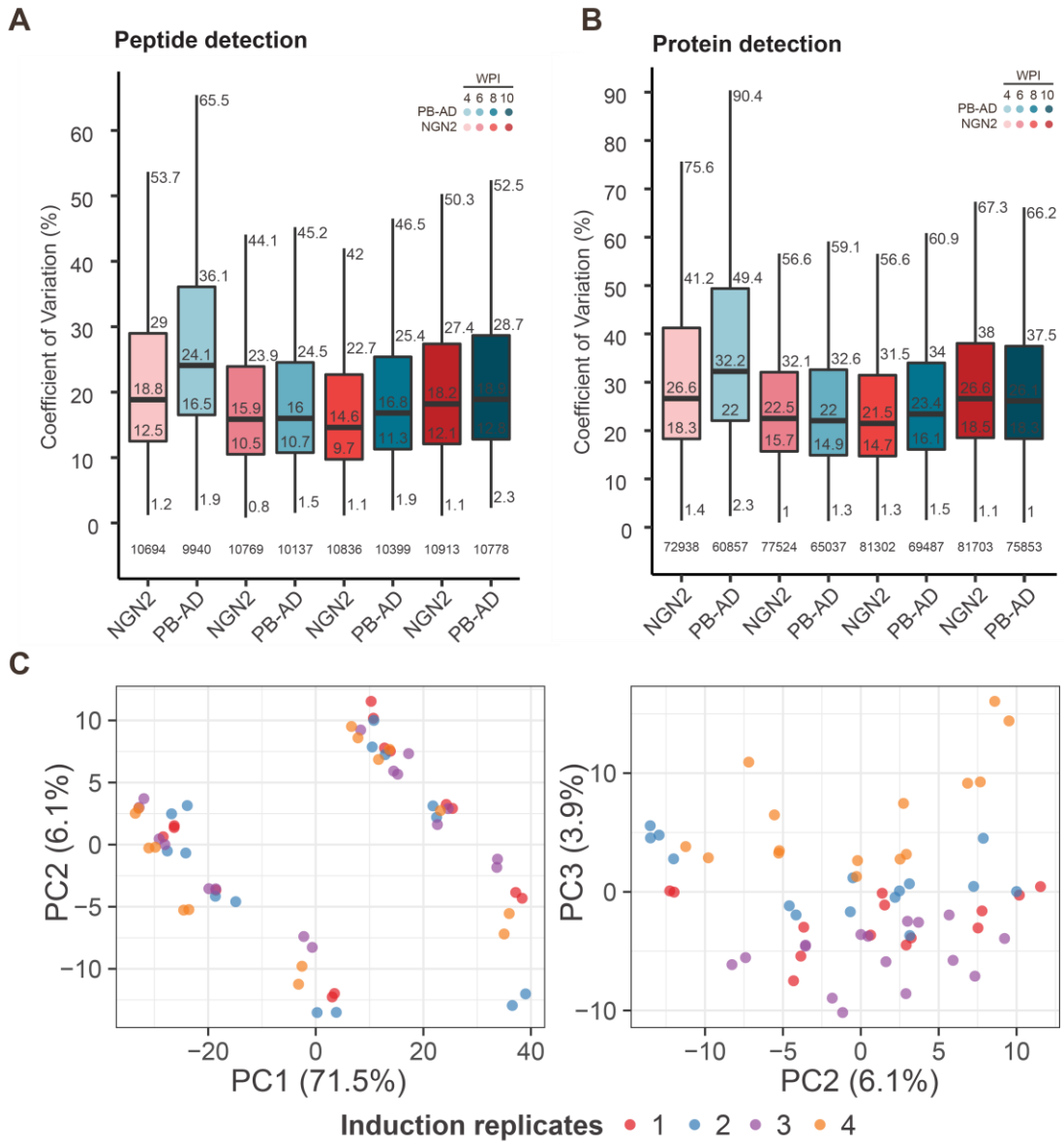

Figure S3. Peptide and protein detection count and variation is similar between cultures and timepoints.

A-B Boxplots showing variation of peptide (**A**) and protein (**B**) detection for all timepoints per culture, indicating median, 1st and 3rd quartiles, and minimum and maximum values. Number of detected peptides and proteins are indicated in the base of the graph. Median coefficient of variation for peptide and protein detection across groups ranged from 14.6% to 32.2%, reflecting consistent detection performance across replicates. **C** PCA plots showing potential batch effects due to induction. PC1 and PC2 show even spread of different inductions but PC3 (3.9%) shows slight separation based on induction and we therefore corrected for induction effect when performing differential abundance analysis.

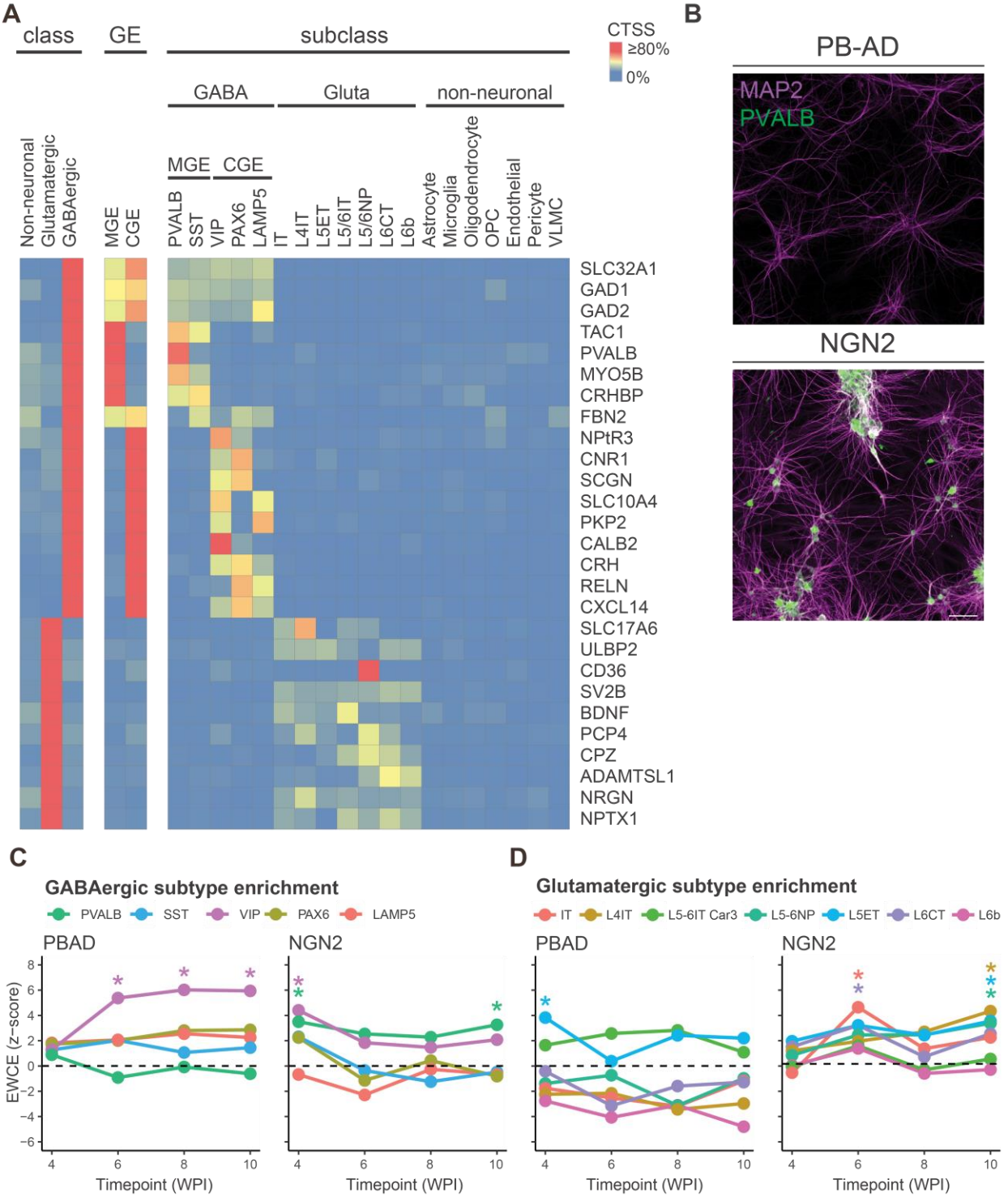

Figure S4. Cell type specificity scores for detected GABAergic proteins

A. Cell type specificity scores (CTSS) scores for detected GABAergic and glutamatergic proteins. CTSS are calculated with the expression weighted cell type enrichment tool (Skene

1409 & Grant, 2016) using single-cell RNA-sequencing data from Jorstad et al. (Jorstad *et al.*, 2023).
1410 MGE and CGE refer to medial and caudal ganglionic eminences. **B.** Representative images of
1411 PB-AD and NGN2 neurons stained for MAP2 and PVALB. Scale bar = 100 μm. **C-D** Expression-
1412 weighted cell type enrichment (EWCE) analysis showing enrichment of proteins higher
1413 expressed in PB-AD or NGN2 for GABAergic **(C)** and glutamatergic subtypes **(D)**. PBAD-
1414 enriched proteins showed strongest enrichment for VIP^+ interneurons at most timepoints,
1415 whereas NGN2-enriched proteins map at different timepoints to both GABAergic ($PVALB^+$
1416 and VIP^+ interneurons) and glutamatergic subtypes. PB-AD-enriched proteins showed
1417 unexpected enrichment for L5ET neurons at 4 WPI, which reduced below significance
1418 threshold at later timepoints. IT and ET refer to intra- and extratelenchephalic-projecting
1419 neurons, and NP refers to near-projecting neurons – cell subclass annotations consistent
1420 with Jorstad et al. (2023) (Jorstad *et al.*, 2023).

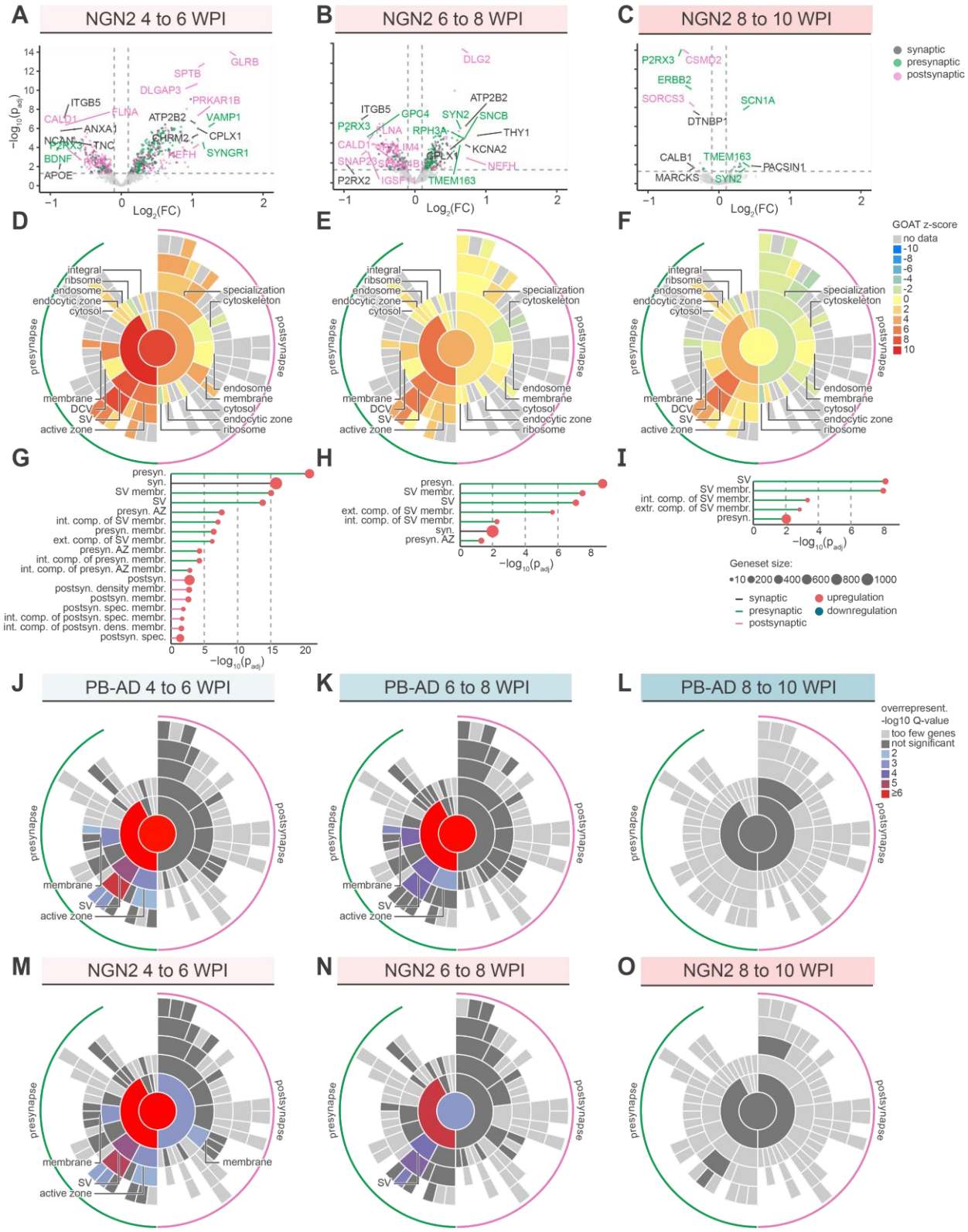
A
NGN2 4 to 6 WPI
B
NGN2 6 to 8 WPI
C
NGN2 8 to 10 WPI
synaptic
presynaptic
postsynaptic
Log2(FC)
D
E
F
GOAT z-score
no data
presynapse
postsynapse
integral
ribsome
endosome
endocytic zone
cytosol
specialization
cytoskeleton
membrane
DCV
SV
active zone
ribosome
G
H
I
Geneset size:
synaptic
presynaptic
postsynaptic
upregulation
downregulation
J
PB-AD 4 to 6 WPI
K
PB-AD 6 to 8 WPI
L
PB-AD 8 to 10 WPI
overrepresent.
-log10 Q-value
too few genes
not significant
M
NGN2 4 to 6 WPI
N
NGN2 6 to 8 WPI
O
NGN2 8 to 10 WPI

1421

1422 **Figure S5. Differential expression of synaptic genes in NGN2 and PB-AD neurons**
1423 **A-C.** Volcano plots showing regulation of synaptic proteins in NGN2 cultures between 6 and
1424 4 (**A**), 8 and 6 (**B**), and 10 and 8 WPI (**C**). Only SYNGO-annotated proteins are plotted and
1425 colour coding refer to significantly regulated synaptic (black) exclusively presynaptic (green)
1426 or postsynaptic (pink) annotations. Proteins were regarded significantly regulated when
1427 adjusted p-value < 0.05 (dashed horizontal line) and $\log_2$ (FC) > 0.1 or < -0.1 (dashed vertical
1428 lines). **D-F**. SYNGO plots showing enrichment scores (z-scores) derived from gene-set
1429 enrichment analysis with GOAT using SYNGO cellular compartment gene sets for 4 to 6 (**D**),
1430 6 to 8 (**E**) and 8 to 10 WPI (**F**). Negative z-scores (blue) reflect enrichments primarily driven
1431 by downregulated proteins and vice versa for positive z-scores (red). **G-I.** Lollipop charts
1432 showing significant SYNGO terms with their corresponding adjusted p-values and the
1433 number of genes part of the gene set. **J-O.** SYNGO overrepresentation analysis of upregulated
1434 proteins in PB-AD (**J-L**) and NGN2 (**M-O**) per timepoint. Foreground are significantly
1435 upregulated proteins and background are all tested genes in corresponding contrast.

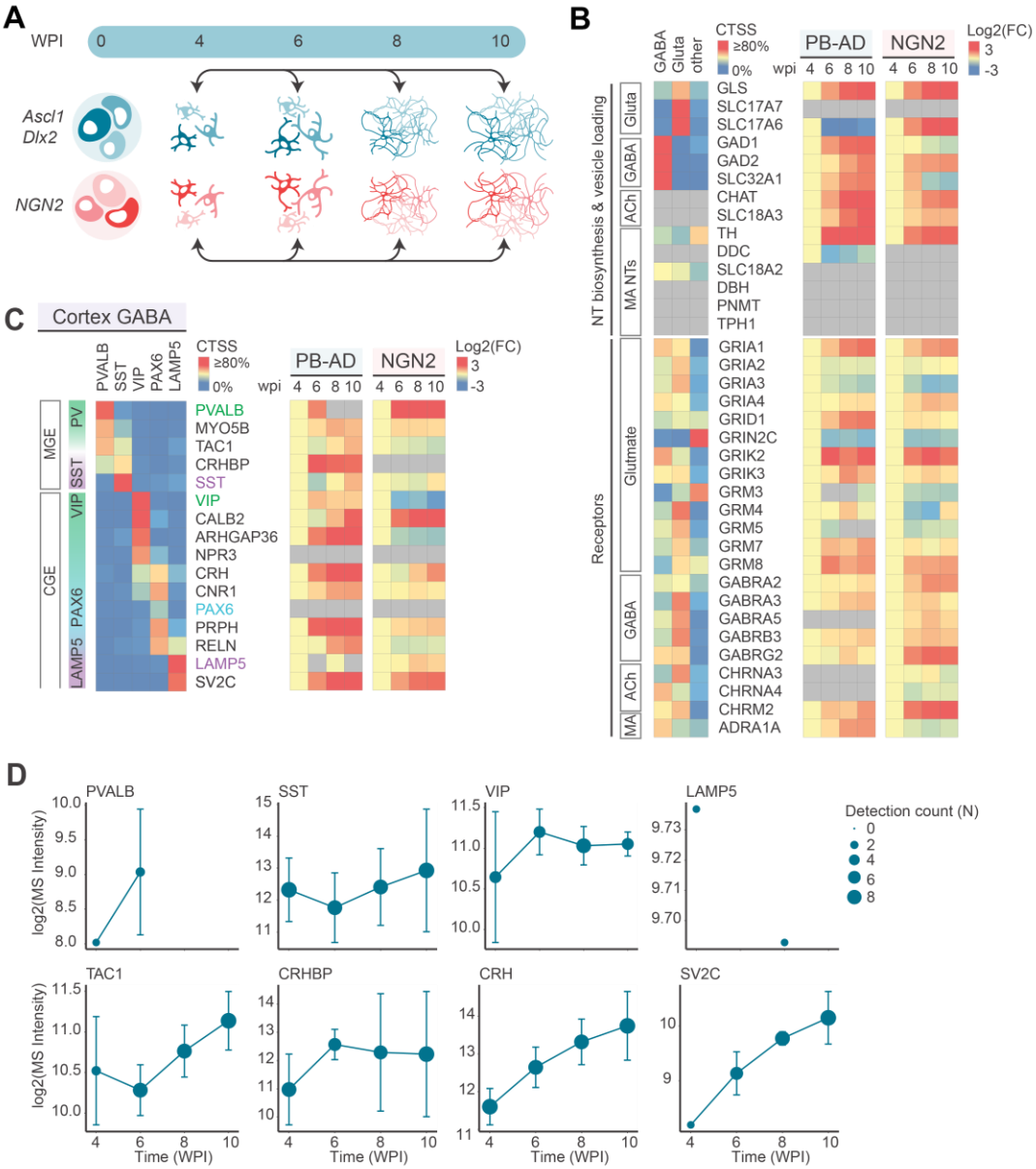

Figure S6. PiggyBac Ascl1/Dlx2 and NGN2 neurons express markers of diverse GABAergic neuron subtypes

A. Contrasts used to determine cell type specification. **B** and **C** Heatmaps that show temporal expression profiles relative to 4 WPI ($\log_2$ (FC)) and cell type specificity scores (CTSS). **B** Typical proteins required for neurotransmitter (NT) synthesis, vesicle loading, and receptors. Undetected proteins are visualized for NT biosynthesis and vesicle loading but not for receptors. **C** Canonical GABAergic subtype markers and proteins with high cell type specificity for GABAergic subtypes and for medial or caudal ganglionic eminences (MGE or CGE). **D.** Line plots show mean expression of canonical GABAergic subtype markers (top) and other

1446 proteins with GABAergic cell type specificity. Error bars represent SD and dot size indicate
1447 detection count.
1448

1449 **Supplemental table 1: SYNGO Proteins with significant expression changes from 8 to 10 WPI**
1450 **in PB-AD neurons**

Protein	new at WPI 10	log_2fc	FDR-adjusted p-value
CNTNAP4	yes	1.05	1.50E-26
SLITRK1	yes	0.97	7.75E-23
CDH1	yes	0.91	4.81E-20
EPHA7	yes	0.90	1.26E-19
ITGB3	no	0.80	1.72E-15
PRRT1	yes	0.74	1.35E-13
NPTX2	no	0.73	4.68E-13
ITGA2	no	0.67	3.46E-11
SLC17A5	yes	0.67	5.09E-11
KCNQ2	yes	0.65	1.77E-10
ELFN1	no	0.65	2.09E-10
CYTH1	no	0.65	2.21E-10
TNC	no	0.64	3.74E-10
NRGN	yes	0.63	6.71E-10
NGDN	yes	0.63	6.73E-10
GPR158	no	0.62	1.43E-09
RELN	yes	0.57	3.53E-08
SCG2	no	0.78	2.18E-03
TMEM163	no	0.62	7.64E-03
PTPRN	no	0.59	2.24E-02
NEFH	no	0.40	2.24E-02
IGSF8	no	0.40	2.24E-02
CNTNAP1	no	0.34	3.78E-02
ATP2B4	no	0.30	3.78E-02

1451